

1

2

3 **A novel mechanism of “metal gel-shift” by histidine-rich Ni²⁺-binding Hpn**
4 **protein from *Helicobacter pylori* strain SS1**

5

6 **Short Title:**

7 Physicochemical aspects of a histidine-rich protein, Hpn

8

9 Rahul Mahadev Shelake¹, Yuki Ito¹, Junya Masumoto¹, Eugene Hayato Morita^{2,3}, Hidenori
10 Hayashi^{1*}

11

12 ¹Proteo-Science Center, Ehime University, Matsuyama, Japan

13 ²Laboratory of Molecular Cell Physiology, Faculty of Agriculture, Ehime University,
14 Matsuyama, Japan

15 ³Department of Chemistry, Faculty of Science, Josai University, Saitama, Japan

16

17 ***Corresponding author:**

18 E-mail: hayashi.hidenori.mj@ehime-u.ac.jp (HH)

19

20

21

22

23 **Abstract**

24 Sodium dodecyl sulphate-polyacrylamide gel electrophoresis (SDS-PAGE) is a universally
25 used method for determining approximate molecular weight (MW) in protein research.
26 Migration of protein that does not correlate with formula MW, termed “gel shifting” appears
27 to be common for histidine-rich proteins but not yet studied in detail. We investigated “gel
28 shifting” in Ni²⁺-binding histidine-rich Hpn protein cloned from *Helicobacter pylori* strain
29 SS1. Our data demonstrate two important factors determining “gel shifting” of Hpn,
30 polyacrylamide-gel concentration and metal binding. Higher polyacrylamide-gel
31 concentrations resulted in faster Hpn migration. Irrespective of polyacrylamide-gel
32 concentration, preserved Hpn-Ni²⁺ complex migrated faster (3-4 kDa) than apo-Hpn,
33 phenomenon termed “metal gel-shift” demonstrating an intimate link between Ni²⁺ binding
34 and “gel shifting”. To examine this discrepancy, eluted samples from corresponding spots on
35 SDS-gel were analyzed by matrix-assisted laser desorption/ionization-time-of-flight mass
36 spectrometry (MALDI-TOF-MS). The MW of all samples was the same (6945.66±0.34 Da)
37 and identical to formula MW with or without added mass of Ni²⁺. MALDI-TOF-MS of Ni²⁺-
38 treated Hpn revealed that monomer bound up to six Ni²⁺ ions non-cooperatively, and
39 equilibrium between protein-metal species was reliant on Ni²⁺ availability. This corroborates
40 with gradually increased heterogeneity of apo-Hpn band followed by compact "metal-gel
41 shift" band on SDS-PAGE. In view of presented data metal-binding and “metal-gel shift”
42 models are discussed.

43 **Key words**

44 Histidine-rich protein; Hpn; nickel; anomalous SDS-PAGE migration; gel shifting on SDS-
45 PAGE; MALDI-TOF-MS; protein-metal ion complex.

46

47 Introduction

48 Cysteine-rich (-SH group) metal-binding proteins, for example metallothioneins, are
49 known to bind and sequester multiple metal ions in prokaryotes and eukaryotes [1], but
50 understanding of histidine-rich (imidazole group) metal-binding proteins is still limited.
51 Proteins with histidine-rich repeats are universally present in the proteomes of both
52 prokaryotes and eukaryotes, including human, and form unique single-residue-repeat motifs
53 [1,2]. *Helicobacter pylori*, a human pathogen responsible for severe gastric diseases including
54 intestinal ulcers and adenocarcinoma, requires two key Ni-containing enzymes (urease and
55 hydrogenase) for survival in acidic gastrointestinal conditions [3]. Thus, *H. pylori* produce
56 unique Ni²⁺-binding histidine-rich proteins required in the maturation of urease and
57 hydrogenase.

58 One of the first candidates involved in Ni²⁺ homeostasis in *H. pylori* was isolated and
59 named Hpn (*Helicobacter pylori* protein binding to nickel) [4]. Hpn contains 28 histidine
60 residues (46.7%) with two stretches of repeated histidines at positions 11-17 and 28-33 (**Fig**
61 **1A**). It also contains two short repeating motifs (EEGCC) in the internal part positioned at
62 38-42 and 51-55. The relative affinity of Hpn towards divalent metal ions was found to be
63 different under *in vivo* and *in vitro* conditions indicating the complex nature of the protein [4–
64 7]. Initial Hpn mutation studies in *H. pylori* showed that the mutant strain was more sensitive
65 to Ni²⁺ than a wild-type strain [4,8,9]. Inductively coupled plasma-mass spectrometry and
66 equilibrium dialysis studies revealed that average five Ni²⁺ ions (5.1±0.2) bind to Hpn in a
67 pH-dependant manner and forms a range of multimeric complexes (>500, 136, 55, 34, 26, 20,
68 14 and 7 kDa) in solution that exists in equilibrium depending on buffer content [5,6]. The
69 pH titration and competition experiments using EDTA confirmed that the metal-binding to
70 Hpn is a reversible process [5–7]. Even though some amino-acid residues vital for metal-
71 binding were identified [10–12], distribution of metal-binding sites and equilibrium between

72 protein-metal species in Hpn is not yet known. Hpn may act in Ni²⁺ storage as a ‘reservoir’ or
73 in channelizing Ni²⁺ to other proteins [5,6,13]. Purified Hpn can form amyloid-like fibers *in*
74 *vitro* [14] but such fibers yet to be established *in vivo* in *H. pylori*. A recent study described
75 Hpn interaction with Hpn-2 (also known as Hpn-like or Hpn-l, another atypical histidine-rich
76 protein with MW 8.07 kDa [15]) mediate urease activity [13]. Thus, considering several
77 complex chemical interactions, Hpn can be employed as an ideal protein to investigate
78 metallochemistry and physicochemical aspects of histidine-rich metal-binding proteins.

79 Even though sodium dodecyl sulfate-polyacrylamide gel electrophoresis (SDS-PAGE)
80 is the most commonly used method for the determination of approximate MW of proteins;
81 unusual electrophoretic behavior in SDS-PAGE has been reported for Hpn, making its
82 identification problematic [5]. This phenomenon of unpredictable migration rate on SDS-
83 PAGE against actual formula MW of protein is termed “gel shift” (not to be confused with
84 the electrophoretic mobility shift assay for protein-DNA interactions). The “gel shifting” has
85 also been reported for several other histidine-rich proteins including Hpn [5], UreE [16],
86 HypB [17–19], SlyD [20,21], Hpn-like [9], and CooC [22] (**Table 1**) as well as different
87 helical membrane proteins [23–25] including some isobaric peptides (peptides with the same
88 MW) from various organisms [26]. HspA from *Helicobacter*, which has a unique C-terminus
89 containing a histidine-rich region, also exhibited a higher MW of 15.5 kDa than the expected
90 13 kDa [27] indicating that the “gel shift” behavior might be attributable to histidine-rich
91 region. However, the molecular mechanism is yet to be clarified. Six possible mechanisms
92 responsible for “gel shifting” of a protein have been hypothesized in previous reports: (a)
93 divergent higher order (secondary or tertiary) structure; (b) difference in Stokes-Einstein
94 (hydrodynamic) radius of the protein-surfactant complex; (c) variation in the intrinsic net
95 charge of the protein; (d) number of bound SDS molecules; (e) post-translational
96 modifications; or (f) binding of cofactors such as metal ions to the protein [23–25,28–30].

97 Nevertheless, polyacrylamide-gel concentration can dictate magnitude and direction of some
 98 proteins in SDS-gel [31].

99 **Table 1. List of histidine-rich Ni²⁺-binding proteins showing gel shifting anomaly.**

Protein	Organism	Function	Histidine content	Ni ions per monomer	Formula MW (kDa)	Apparent MW (kDa)	Reference
SlyD	<i>Escherichia coli</i>	Ni carrier	10.2%	3	20.8	25	[20,21]
CooC	<i>Rhodospirillum rubrum</i>	Nickel accessory protein for maturation of CODH	3%	1	27.8	61, 29	[22]
HypB	<i>Rhizobium leguminosarum</i>	GTP-dependent Ni insertase	9.0%	4	32.5	39	[18,19]
HypB	<i>Archeoglobus fulgidus</i>	GTP-dependent Ni insertase	2.7%	0.5	24.7	41 (dimer)	[17]
UreE	<i>Klebsiella aerogenes</i>	Accessory protein in urease maturation	9.5%	3	17.5	35 (dimer)	[16]
Hpn like	<i>Helicobacter pylori</i>	Ni storage	25%	2	9	47, 18	[9]
Hpn	<i>Helicobacter pylori</i>	Ni storage	46.7%	5-6	7	>670, 500, 230, 136, 20, 14, 7	Present study and [5]

100

101 Recently, attempts have been made to investigate these molecular mechanisms using
 102 segments of various membrane proteins, and the findings indicated that there might be no
 103 single universal mechanism that accounts for the anomalous migration of all proteins. In fact,
 104 each protein or class of proteins may have unique chemistry responsible for “gel shifting”
 105 behavior. It is an interesting question that whether “gel shifting” in Hpn is linked to the
 106 displacement of protein-protein, protein-metal, and/or protein-SDS interactions, but these
 107 need further investigation.

108 We cloned the *hpn* gene from the Sydney Strain 1 (SS1) of *H. pylori*, a standardized
 109 mouse model [32]. Our preliminary data demonstrated the altered migratory position for Hpn
 110 on SDS-PAGE when Hpn was expressed in Ni²⁺-supplied medium suggesting role of Ni²⁺ in
 111 altered migration. We find that the migration rate of Ni²⁺-treated Hpn on SDS-PAGE was

112 altered because of preserved protein-metal complexes. Preservation of intact protein-metal
113 bond in non-denaturing conditions is commonly reported [33,34]. SDS-PAGE is primarily
114 designed to separate denatured proteins by disrupting non-covalent complexes. However, in
115 SDS-treated samples, protein under study and proteins used as MW standards attain
116 equivalent shape not by an absolute unfolding but indeed it is achieved by the SDS
117 aggregation at hydrophobic sites [23]. Thus, protein denaturation occurs in “reconstructive”
118 manner and it forms a mixture of SDS micelle wrapped around α -helices separated by linkers
119 (necklace and bead model) or hydrophobic regions of protein wrapped around SDS micelles
120 (decorated micelle model), both reviewed in [35]. Thus, some SDS-resistant protein-protein
121 interactions (**supporting information, S1 Table in S1 file**) and protein-metal complexes
122 (**supporting information, S2 Table in S1 file**) can also preserve in electrophoretic separation
123 upon SDS-PAGE provided interaction is stronger [34]. Also, many studies reported that the
124 “reconstructive” denaturation can retain some protein-metal complexes on SDS-PAGE but
125 altered migration is not generally observed except for some Ca^{2+} -binding proteins such as
126 calmodulin isoforms [36] and Ca^{2+} -dependent protein kinases (CDPKs) [37–40]. Overall, the
127 above observations suggest that there may be an apparent link between metal-binding to Hpn
128 and “gel shifting” pattern. Thus, the anomalous migration of Hpn should be explored in
129 several conditions pertaining to metal binding and its effect on migration rate in SDS-PAGE.
130 Also, MW of intact Hpn alongside protein-metal interaction studies by MS could facilitate
131 better understanding of Hpn metallochemistry in detail.

132 In the present study, an attempt was made to investigate various physicochemical
133 properties of Hpn and not the *in vivo* function of Hpn in *H. pylori* itself. This work was
134 focused on heterologous expression of Hpn in *E. coli*, average molecular mass of purified
135 Hpn, “gel shifting” anomaly with or without Ni^{2+} in different polyacrylamide-gel
136 concentrations and application of MALDI-TOF-MS for studying non-covalent Hpn- Ni^{2+}

137 complexes. To establish a reliable technique to determine MW associated with “gel shifting”
138 anomaly without ambiguity, MW of intact recombinant Hpn was determined by MALDI-
139 TOF-MS using internal protein standards and found to be essentially identical (6945.66 ± 0.34)
140 to the formula MW. Ni²⁺-treated Hpn migrated more rapidly than untreated Hpn showing
141 differences of 3-4 kDa. This significant metal-triggered shift in electrophoretic gel mobility
142 of Hpn is reported for the first time to the best of our knowledge and termed as a “metal gel-
143 shift”. Migration speed of Hpn in both the forms was altered depending on polyacrylamide-
144 gel concentrations. The method for sample and matrix preparation standardized in this study
145 preserved appropriate intermolecular interactions and hence boosts the usefulness of MALDI
146 for the study of non-covalent protein-metal ion complexes.

147

148

149

150

151

152

153

154

155

156

157

158

159

160 **Materials and Methods**

161 ***H. pylori* strain and growth conditions**

162 All the chemicals and reagents used were of analytical grade or higher. The mouse-
163 adapted strain of *Helicobacter pylori* Sydney strain (*H. pylori* SS1) was used in this study
164 [32]. *H. pylori* SS1 was grown on Trypticase Soy agar with 5% sheep blood (TSA II) (Becton
165 Dickinson, Franklin Lakes, NJ) for three days at 35°C in 12% carbon dioxide condition. A
166 single colony was isolated and sub-cultured on TSA II agar at 35°C in 12% carbon dioxide
167 condition.

168 **Purification of DNA from *H. pylori* strain SS1**

169 The genomic DNA from strain SS1 was extracted based on phenol-chloroform
170 method as described previously [32] with minor modifications. Briefly, bacteria were
171 harvested from TSA II agar and suspended in 3 ml of Tris-buffered saline (TBS). After
172 washing with TBS once by centrifugation at 3,800 g for 5 min at 4°C, 5×10^8 colony forming
173 unit (CFU) of bacteria were re-suspended in 500 μ l of lysis buffer (50 mM Tris-HCl, pH 8.0;
174 100 mM EDTA, pH 8.0; 1 % SDS, 100 mM NaCl) containing 0.2 mg/ml proteinase K
175 (Amaresco, Solon, OH) and incubated at 37°C for 12 h. Subsequently, UltraPure™ buffer-
176 saturated phenol (Invitrogen, Carlsbad, CA) was added, and the mixture was gently rotated
177 for 15 min. After centrifugation, the aqueous phase was transferred to a tube containing
178 chloroform/isoamyl alcohol (24:1, Sigma-Aldrich, St. Louis, MO) and agitated gently for 10
179 min. The aqueous phase was collected to a new tube by centrifugation. The DNA was
180 precipitated by addition of isopropyl alcohol and 0.3 M sodium acetate, and then the DNA
181 pellet was rinsed with 70% ethanol. After centrifugation, pellet was air-dried and dissolved in
182 Tris-EDTA buffer (pH 8.0).

183 **Cloning and nucleotide sequencing**

184 First, the Hpn encoding region of 1.17 kb was amplified instead of the *hpn* gene only
185 to avoid undesired mutations in the nucleotide sequence of *hpn* (primers 5'-
186 AGTCCATATGCCTTACACGCCGTAGATGACAAAACGCGC-3' and 5'-
187 GACTGGATCCGGCTCGCTCTCATCTATAGCGTGGCTAAG-3'). The DNA fragment was
188 cloned into a pBluescript II KS (+) vector (Takara, Japan), and nucleotide sequencing was
189 performed using a BigDye Terminator v3.1 Cycle Sequencing Kit and an ABI PRISM 310
190 Genetic Analyzer (Applied Biosystems). The *hpn* gene was amplified using the cloned 1.17
191 kb region as the PCR template (primers 5'-
192 GACTCATATGGCACACCATGAAGAACAACAC-3' and 5'-
193 GACTGGATCCTTATTACTCGTGATGCCCGTGGC-3') and then cloned into pBluscript
194 (Takara, Japan) and pET21b (Novagen, Darmstadt, Germany) vectors. *E. coli* JM 109 and
195 BL21 (DE3) cells purchased from Takara (Japan) were used for the propagation and protein
196 expression with a constitutive (RuBisCo promoter from *Synechococcus* sp. PCC7002) [41];
197 and isopropyl β -D-1-thiogalactopyranoside (IPTG)-inducible T7 promoter, respectively.

198 **Expression and purification of recombinant Hpn**

199 Recombinant Hpn was purified from harvested cells of 200 ml culture. Harvested
200 cells were suspended in lysis buffer (50 mM Tris-HCl, pH 7.5, and 500 mM NaCl) and
201 purification was done as described previously for His-tagged proteins with some
202 modifications [42]. After sonication (TOMY Ultrasonic Disruptor, duty: 50, output: 4, time: 4
203 min x 6), supernatant fractions were filtered using Millex[®] GV filter units of 0.22- μ m-pore-
204 size and applied onto a 1-ml HiTrap chelating column (GE Healthcare) that had been
205 equilibrated with start buffer containing 20 mM imidazole, 50 mM Tris-HCl, and 500 mM
206 NaCl. The column was washed with buffer (50 mM Tris, pH 7.5, 50 mM NaCl, and 40 mM
207 imidazole), and then Hpn was eluted using start buffer with 400 mM instead of 20 mM
208 imidazole. Eluted fractions were analyzed for purity using SDS-PAGE (15%), and the purest

209 fractions were applied onto a 5-ml HiTrap desalting column (GE Healthcare) that had been
210 equilibrated with desalting buffer (20 mM Hepes-KOH, pH 7.4, 100 mM NaCl, and 20%
211 glycerol), and purified Hpn was stored at -80°C until use. The concentration and quality of
212 purified Hpn was measured using bovine serum albumin (BSA) as the standard in a BCA
213 assay (Bio-Rad) in accordance with the manufacturer's instructions and SDS-PAGE
214 (polyacrylamide 15%), respectively.

215 **SDS-PAGE and non-denaturing native-PAGE (native-PAGE)**

216 All purified protein fractions were analyzed by SDS-PAGE in accordance with
217 instructions mentioned previously [43]. A vertical electrophoresis system of mini-slab size
218 from Atto Co. (Japan) was used for the separation of protein samples with appropriate
219 concentrations of polyacrylamide. A LMW-SDS Marker Kit (GE Healthcare) and marker
220 proteins kit from Nacalai Tesque, Inc. (Japan) were used as protein standards in SDS-PAGE.
221 All protein samples were prepared in Laemmli buffer (50 mM Tris-HCl pH 6.8, 10% glycerol,
222 2% SDS, 7% β -mercaptoethanol and 0.001% bromophenol blue) and then stored at -20°C
223 before use. The electrophoresis was done till bromophenol blue dye reached to the bottom in
224 all gels of different concentrations (under similar experimental conditions). This optimized
225 method was referred from previous work [31] showing separation of 11 trans-membrane
226 mimetic peptides, translating into MWs of 3.5-41 kDa on 11-18% of polyacrylamide-gel.
227 Resolved proteins were stained with Coomassie Brilliant Blue (CBB) R-250 solution
228 containing 10% acetic acid with 25% methanol.

229 Fractions of purified Hpn were used for blue native PAGE analysis without boiling or
230 reduction in sample buffer (50 mM Tris with pH 6.8 containing 0.01% bromophenol blue and
231 10% glycerol). The running buffer was prepared without detergent and consisted of 25 mM
232 Tris, 192 mM glycine, pH 8.0. Stacking gel (4%) and separation gel (10%) were prepared
233 adding suitable buffers, glycerol, ammonium persulfate (APS), and TEMED. Electrophoresis

234 was performed at a constant current of 15 mA and voltage of 160 V and further CBB stained.

235 **Western blotting analysis**

236 The Hpn protein (25 μ M) treated with indicated mol equivalent of EDTA or Ni²⁺
237 resolved on SDS-PAGE (20%) and then electrophoretically blotted onto polyvinylidene
238 fluoride (PVDF) membrane (Amersham Hybond-P, GE Healthcare, code: RPN303F) in
239 transfer buffer containing no methanol. Blotting was performed at 0.8 mA current for every
240 cm² area of gel. Proteins were blocked on PVDF membranes in a solution of 5% skim milk
241 for 1 h after washing in PBS-T buffer (phosphate-buffered saline buffer with 0.05% Tween-
242 20, pH 8). The PVDF membrane was further incubated with C-terminal specific-anti
243 6 \times histidine monoclonal antibody (9F2) (Wako Japan, product code: 010-21861 diluted to
244 1:5000 in PBS-T) for 1 h. After three washes of 15:5:5 min in PBS-T, PVDF membrane was
245 then incubated with horseradish peroxidase-conjugated anti-mouse IgG (GE Healthcare,
246 product code: NA931VS, diluted to 1:5000 in PBS-T) for 1 h. The membrane was further
247 washed again with PBS-T as mentioned earlier and Amersham ECL non-radioactive western
248 blotting detection reagents (GE Healthcare) were used for visualizing protein bands in
249 accordance with the manufacturer's instructions.

250 **Enzyme-linked immunosorbent assay (ELISA) analysis**

251 Green fluorescent protein with artificial His.tag (*gfp-His₆*) and GFP fused with Hpn (*gfp-*
252 *Hpn*) were cloned in pET21b. IPTG-induced over-expression of both the proteins was done
253 with or without Ni²⁺ added in the culture (**Supporting information, S1 Fig in S1 file**).
254 Pellets of 60 μ l bacterial cultures were dissolved in 60 μ l sample buffer and incubated for 3
255 min at 100°C. Final volume of 15 μ l loaded in each lane for SDS-PAGE. ELISA experiment
256 was performed using previously described protocol with some modifications [44]. Different
257 buffers were prepared before starting ELISA experiment (components of buffers summarized
258 in Table 2).

259 **Table 2. Components of different buffers used in ELISA.**

260

Buffer type	Components
Coating buffer	Phosphate buffer saline, [1.16 g Na ₂ HPO ₄ , 0.1 g KCl, 0.1 g K ₃ PO ₄ , 4.0 g NaCl (500 ml distilled water) pH 7.4]
Dilution buffer	0.1% BSA with 0.05% Tween-20 in PBS
Blocking buffer	1% BSA with 0.05% Tween-20 in PBS
Washing buffer	0.05% Tween-20 in PBS
Stop buffer	5N Sodium Hydroxide in distilled water

261

262 Flat-bottom 96-well ELISA plates (untreated 96-well microplates from Falcon) were
263 used for coating. Concentration of each protein (Hpn, GFP-Hpn and GFP-His₆) was adjusted
264 to 1 µg by dilution with coating buffer to the final volume of 50 µl. Plates were incubated at
265 4°C for overnight. Next day, solution was thrown away and 200 µl blocking buffer into each
266 well was added. Then, plate was incubated at 37°C for 1hr. After incubation, solution was
267 discarded and plate was washed three times by washing buffer. His.Tag® antibody was
268 diluted to standardized concentration (1:500) with dilution buffer [C-terminal specific-anti
269 6xhistidine monoclonal antibody (9F2) (Wako Japan, product code: 010-21861)] and plate
270 incubated at 37°C for 1hr after adding 100 µl in each well. After three washes with wash
271 buffer, plate was incubated with horseradish peroxidase-conjugated anti-mouse IgG (GE
272 Healthcare, product code: NA931VS, diluted to 1:1000 in wash buffer) for 1 hr at 37°C. After
273 similar washing, the substrate ABTS [2,2'-Azinobis(3-ethylbenzothiazoline-6-sulfonic Acid
274 Ammonium Salt) from Wako Japan] dissolved in 0.1 M citrate buffer and hydrogen peroxide
275 (0.03%) was added. Then the plate was incubated for 20 minutes at room temperature.
276 Reactions were stopped by adding stop buffer (100 µl) in each well. The absorbance at 415
277 nm was measured using a Spectramax M3 microplate reader (Molecular Devices Co.,
278 Sunnyvale, CA). Values obtained (absorbance at 415 nm) for Ni²⁺-treated samples (from

279 average of at least three replications) were normalized against untreated samples and plotted
280 in graph.

281 **Hpn interaction with Ni²⁺ ions**

282 For SDS-PAGE and blue native-PAGE analysis, apo-Hpn (25 μM) was prepared as
283 mentioned above and then treated with the indicated amount of Ni²⁺ by adding NiSO₄
284 solution or EDTA (with mol equivalent ratio of 1:6) and incubated for a minimum of 1 h at
285 room temperature. Suitable PAGE buffer was added to the above mixture for loading either
286 on SDS-PAGE (Laemmli buffer) or blue native PAGE (sample buffer used, 50 mM Tris, pH
287 6.8 with 10% glycerol and 0.01% bromophenol blue). Equal volume of 2X loading buffer
288 was added to protein samples and then applied to native-PAGE directly. For SDS-PAGE,
289 further processing (heat denaturation) done otherwise mentioned in respective figures. Ni²⁺
290 binding to Hpn protein was investigated using MALDI-TOF-MS by mixing Ni²⁺ or EDTA-
291 treated Hpn with equal amount of matrix solution.

292 The gel slices of EDTA or Ni²⁺-treated protein bands resolved on SDS-gel were
293 digested in nitric acid (Nacalai Tesque, Japan) and heated at 80°C for 10 min, once cooled
294 nitric acid finally diluted to 2%. The Ni²⁺ content was analyzed by ICP-optical emission
295 spectrometry (ICP-OES) (Optima 8300 ICP-OES Spectrometer, PerkinElmer Inc, USA). The
296 standard curve was plotted using a minimum of five standards (ranging from 50 to 1000 ppm)
297 with a blank of 2% nitric acid.

298 **MALDI-TOF-MS**

299 Protein bands resolved on SDS-PAGE were eluted using the protocol described
300 previously [45] with or without CBB staining and then aliquots were used in mass
301 spectrometry. Purified Hpn and elution fractions were directly mixed with an equal volume of
302 matrix solution prepared with different recipes. Acidic and non-acidic matrices were
303 investigated for detecting intact protein-metal ion complexes. Acidic matrix was prepared by

304 mixing 100% acetonitrile (ACN), 0.1% trifluoroacetic acid (TFA), and distilled water (v:v,
305 50:10:40). Another mild acidic matrix was prepared with the recipe except for more diluted
306 0.01% TFA. Two different non-acidic matrices were analyzed: 1) sinapinic acid in 100%
307 ACN and distilled water (v:v, 1:1) without TFA [46]; and 2) 4-hydroxy- α -cyanocinnamic acid
308 powder in a saturated solution of ethanol and 1 M ammonium acetate (v:v, 1:1) [47].
309 MALDI-TOF-MS analysis was done with a Voyager-DE PRO MALDI-TOF-MS (Applied
310 Biosystems). The instrument was calibrated externally with a Sigma Protein MALDI-MS
311 calibration kit. The positive linear mode was set in the instrument to acquire mass spectra
312 using a nitrogen laser (337 nm). An average of a minimum of 150 laser shots was used to
313 accumulate a single spectrum with an accelerating voltage of 25,000 V and extraction delay
314 time of 400 ns. Internal calibration with protein standards (insulin and apomyoglobin),
315 smoothing and baseline correction of the mass spectra was performed and analyzed by using
316 Data Explorer software (Applied Biosystems, MA).

317 **Effect of Ni²⁺ on growth of *E. coli* expressing the *hpn* gene**

318 *E. coli* cultures, both with pBluscript only and pBluscript-*hpn* plasmid inoculated
319 from individual colonies were grown for overnight in Luria-Bertani (LB) medium containing
320 100 μ g/ml ampicillin at 37°C. Optical density (OD) of the grown cultures was measured at
321 600 nm and normalized to 1, of which 100 μ l was inoculated to 5 ml of fresh LB medium
322 (1:50 dilution) containing 100 μ g/ml ampicillin, and NiSO₄ was added where applicable (0,
323 500, 1000, 1200 μ M). Cultures were grown for 4 h at 165 rpm at 37°C, OD values were
324 measured using U-1800 spectrophotometer (Hitachi, Japan) at 600 nm. Obtained values were
325 normalized against control (culture grown without Ni²⁺ stress) and data from three different
326 replicates was summarized and used to plot the growth curve.

327 M9 medium is a minimal defined culture medium prepared as described previously
328 [48]. Overnight grown cultures (as above, 100 μ l) were inoculated into 5 ml of fresh M9

329 medium containing 0, 50, and 100 μM NiSO_4 and 100 $\mu\text{g/ml}$ ampicillin. These cultures were
330 incubated for 24 h at 165 rpm at 37°C in a shaker and the growth curve was plotted (as
331 described above).

332 **Ni^{2+} accumulation in *E. coli* expressing the *hpn* gene**

333 Single colonies of transformed *E. coli* JM109 were inoculated into 2 ml of fresh
334 medium (LB or M9) supplemented with appropriate concentrations of Ni^{2+} . Overnight grown
335 cultures (after normalizing OD to 1) were inoculated into 5 ml of fresh medium and grown
336 for 24 h at 37°C with and without Ni^{2+} . Sampling (2 ml culture) was done at 24 h (LB and
337 M9), respectively. Cells were centrifuged at 15000 rpm for 1 min and bacterial pellet was
338 washed with GET buffer (50 mM glucose, 25 mM Tris-HCl, 10 mM EDTA) followed by
339 drying at 80°C for a minimum of 3 h. The dried pellet was digested in nitric acid (Nacalai
340 Tesque, Japan) and heated at 80°C for 10 min, once cooled nitric acid finally diluted to 2%.
341 The Ni^{2+} content incorporated inside the cell and total uptake were analyzed by ICP-OES.

342

343

344

345

346

347

348

349

350

351

352

353

354 Results

355 Overexpression and purification of Hpn

356 Four changes were observed at the nucleotide level in the *hpn* ORF of strain SS1
357 compared with strain 26695, but it had no change at the amino-acid level (**Supporting**
358 **information, S2 Fig in S1 file**). Hpn expression in *E. coli* culture was standardized in LB
359 medium. The molecular mass of Hpn expressed with and without Ni²⁺ was investigated by
360 SDS-PAGE with a crude cell extract and found to be different (**Fig 1B**). The SDS-PAGE
361 pattern of imidazole-eluted Hpn showed three major protein bands of approximately 14 kDa,
362 18 kDa, and 70 kDa on 15% polyacrylamide-gel (**Fig 1C**). The SDS-resistant oligomeric
363 complex (~70 kDa) was highly stable and unaffected by reducing agents such as β-
364 mercaptoethanol or boiling (100°C for 3 min). After desalting, this ~70 kDa band was
365 observed but at very low concentration, thereby suggesting the role of imidazole in inter-
366 conversion of Hpn multimeric forms (**Fig 1D**). The other two protein bands of ~14 kDa and
367 ~18 kDa were observed corresponding to the pattern of the crude extract with and without
368 Ni²⁺ respectively. This indicates that a trace of Ni²⁺ was present in purified Hpn incorporated
369 during the purification process. Thus, the purified Hpn was used after removing trace
370 amounts of Ni²⁺ by treating with EDTA during buffer exchange with desalting columns (**Fig**
371 **1E**).

372

373 **Fig 1. Amino acid sequence, overexpression and purification of recombinant Hpn.**

374 Lane M, LMW protein marker standards (GE Healthcare); black arrows depicting apo-Hpn
375 and white arrows showing probable Ni²⁺-bound Hpn protein in all panels.

376 A. Amino acid sequence of Hpn. Histidine residues are highlighted in bold. Stretches of six
377 and seven histidines are highlighted in green and pentapeptide repeats (EEGCC) are
378 underlined.

379 B. SDS-PAGE of Hpn expression with or without Ni²⁺ added in the culture (polyacrylamide-

380 gel 20%). Pellets of 60 μ l bacterial cultures were dissolved in 60 μ l of 1X Laemmli buffer
381 and boiled for 3 min at 100°C. Final volume of 15 μ l loaded in each lane.

382 C, D and E. Elution profile of purified Hpn checked by loading protein fractions on SDS-
383 PAGE (polyacrylamide-gel 15%). Lanes 1 to 10, fractions of purified protein eluted with 400
384 mM imidazole (C). Elution profiles of desalted fractions of Hpn without EDTA treatment (D)
385 and with EDTA-treatment (E) were analyzed. Equal volume of 2X Laemmli buffer was added
386 to each eluted fraction and then boiled for 3 min at 100°C. Total 10 μ l applied in each lane in
387 C, D and E.

388

389 It has been shown that Hpn forms a range of multimeric complexes depending on
390 buffer composition and treatment of DTT, imidazole and Ni^{2+} estimated by gel-filtration
391 chromatography [5]. Consistent with earlier report, Hpn protein (25 μ M) treated with either
392 EDTA or Ni^{2+} (mol equivalent ratio of 1:6 independently) migrated as a range of multimeric
393 species on 10% native-PAGE gel (**Supporting information, S3Fig in S1 file**).

394 **Confirmation of recombinant Hpn by Western blotting**

395 The post-translational removal of N-terminal methionine (149.21 Da) in wild-type (in
396 *Helicobacter pylori*) and recombinant Hpn (in *E. coli*) is reported [4,5]. Therefore, the
397 monoisotopic and average molecular mass (abbreviated as M_{MONO} and M_{av}) of Hpn without
398 N-terminal methionine were estimated using PAWS software (<http://www.proteometrics.com>)
399 as 6941.288 Da and 6946.01 Da, respectively. Hpn appeared to migrate faster in the sample
400 from cells cultured with Ni^{2+} compared to that without Ni^{2+} on 15% (**Fig 1C-E**) or 20% SDS-
401 PAGE (**Fig 1B**), but neither of the conditions showed the migratory position for an expected
402 MW i.e. ~7 kDa.

403 To facilitate the identification of Hpn protein (untagged) precisely, western blotting
404 was performed using a His.Tag[®] monoclonal antibody assuming that the His.Tag[®] antibody
405 would bind to Hpn at the seven and six residue histidine repeats [5]. Recombinant Hpn
406 (untagged) confirmed a thin band in western blot (**Fig 2A**, left panel) corresponding to the

407 migration position of apo-Hpn but Ni²⁺-treated Hpn was barely visible. CBB staining of same
408 PVDF membrane showed both the protein bands but small amount of Ni²⁺-treated Hpn
409 remain bound to membrane (**Fig 2A**, right panel). Possible explanation is that untagged Hpn,
410 specifically metalated form may have weaker binding affinity to membrane probably due to
411 its atypical chemical nature.

412

413 **Fig 2. Western blot and ELISA analysis of Hpn, GFP-His₆ and GFP-Hpn.**

414 A. Western blot of Hpn was done using His.Tag[®] monoclonal antibody. In left panel, X-ray
415 sheet showing ECL detection result of recombinant Hpn (with and without Ni²⁺) and right
416 panel showing same CBB-stained-PVDF membrane used for ECL detection.

417 B. Western blot of untagged Hpn, GFP-Hpn and GFP-His₆ on PVDF membrane either treated
418 with or without Ni²⁺ solution (1mM of NiSO₄).

419 C. ELISA of denatured untagged Hpn, GFP-Hpn and GFP-His₆ Equal amount of protein (1
420 µg) was coated on ELISA plate. His.Tag[®] antibody was diluted to 1:500 for detection. Values
421 obtained (absorbance at 415 nm) for Ni²⁺-treated samples (from average of at least three
422 replications) were normalized against untreated samples and plotted in graph. Paired t-test
423 was performed to compare the metal ion effect, ** indicate p<0.01.

424

425 **Metal-binding to Hpn changes Hpn-antibody interaction**

426 Interaction of His.Tag[®] antibody with Hpn may not necessarily show similar results
427 for other protein having artificial His.Tag or Hpn conjugated with another protein owing to
428 differential co-ordination geometry of metal-binding and its chemical surrounding. We
429 investigated this possibility using GFP- His₆ and GFP-Hpn (**Fig 2B**). GFP does not interact
430 with His.Tag[®] antibody by its own. GFP is comparatively large protein (26.7 kDa) but still
431 positional shift was observed in case of GFP-Hpn expressed in LB medium supplied with
432 Ni²⁺. Western blot data of GFP-His₆ and GFP-Hpn showed almost equal intensity signals in
433 both the cases i.e. with or without Ni²⁺.

434 Recognition site for His.Tag[®] antibody is His₆ peptide attached at C-terminal of a

435 recombinant protein and it is a linear epitope. Hence, conformational change upon Ni^{2+} -
436 binding to Hpn may lead to altered binding of His.Tag® antibody. This was further examined
437 by ELISA using His.Tag® antibody (**Fig 2C**). The SDS-treated and non-treated Hpn protein
438 shown similar results which is compatible with previous observations for several other
439 proteins [49,50]. The relative detection sensitivity of Ni^{2+} -treated protein with His.Tag®
440 antibody in ELISA give order of untagged Hpn < GFP-Hpn < GFP-His₆. Hence, the
441 variability that we observed in detection of apo- and metalated-Hpn on western blots may
442 have resulted not only from membrane-binding efficiency but also from differential exposure
443 of His-rich region upon metal-binding.

444 These data signify that the metal-binding to Hpn causes altered binding of His.Tag®
445 antibody, possibly due to change in protein confirmation.

446 **Determination of MW by MALDI-TOF-MS**

447 To quantify the reliable molecular mass of untagged Hpn, MALDI-TOF-MS was used
448 for purified apo-Hpn with an acidic matrix in linear positive mode. As shown in **Fig 3A**,
449 integral signals of four heteromeric species of Hpn (M^+ , 2M^+ , 3M^+ , and 4M^+) were observed
450 with a major peak of singly charged Hpn[M^+]. Although a tendency of apo-Hpn to form
451 multimeric complexes in native and reduced states was confirmed by native-PAGE and SDS-
452 PAGE (with 400 mM imidazole-buffer), respectively, the appearance of a major peak of
453 monomer and low intensity peaks of heteromeric species in MALDI-TOF-MS analysis is of a
454 great advantage in determining the molecular mass accurately.

455 Insulin (M_{MONO} 5729.6009; M_{av} 5734.51) and apomyoglobin (M_{MONO} 16940.9650;
456 M_{av} 16951.49) were used as internal standards for mass calibration while acquiring spectra.
457 The M_{av} of Hpn was determined as 6945.66 ± 0.34 Da calculated from the average of at least
458 five different measurements. A representative calibrated peak of Hpn[M^+] with m/z 6946.05 is
459 shown in **Fig 3B**. However, MALDI-TOF-MS analysis confirmed that the M_{av} of purified

460 recombinant Hpn was 6945.66 ± 0.34 Da instead of the calculated molecular mass of 7,077 Da.
461 This suggests the loss of the N-terminal methionine residue (m/z 149.21), probably in post-
462 translation process in *E. coli* and this observation is consistent with the previous reports [4,5].

463

464 **Fig 3. Molecular mass analysis of Hpn with MALDI-TOF-MS.**

465 A. Sharp peak of monomeric Hpn together with neighboring small peak of matrix adduct, and
466 three oligomeric species with lower intensity was observed in Hpn spectrum. The monomeric
467 and three oligomeric species: M^+ , $2M^+$, $3M^+$, and $4M^+$ with masses of m/z 6942.09, 13874.39,
468 20807.59, 27740.62 respectively are shown in inset.

469 B. Molecular mass of Hpn was measured (m/z 6946.05) using two different internal standards
470 (insulin and apomyoglobin), which showed peaks for protonated and doubly charged species.
471 Average MW of recombinant Hpn (without methionine) determined (6945.66 ± 0.34) is
472 showing almost negligible difference (0.35) compared to theoretical MW (6946.01).

473

474 **Hpn exhibits both “gel shifting” and “metal gel-shift”**

475 The reduction by β -mercaptoethanol and boiling before gel loading of purified Hpn
476 had no effect on the appearance of two bands even in different polyacrylamide-gel
477 concentrations [(~14 kDa and ~18 kDa on 15% SDS-PAGE; **Fig 1C-E**) and (~7 kDa and <7
478 kDa on 20% SDS-PAGE; **Fig 4A**)]. This was further analyzed by Ni^{2+} addition and removal
479 (using EDTA) separately to the purified Hpn. In both cases, samples with and without boiling
480 were analyzed in order to assess if Hpn showed a characteristic property of “heat
481 modifiability” like outer membrane proteins (OMPs) from *E. coli* [51]. The concept of heat
482 modifiability constitutes preservation of both folded and unfolded structures upon SDS
483 treatment to purified OMPs but with no heat and shows two different bands on SDS-PAGE.
484 Heating denatures the folded β -content of OMPs and SDS-PAGE data shows single band. No
485 difference in migration pattern was observed between heated and non-heated samples of Hpn
486 indicating the absence of heat modifiability (**Fig 4A**).

487 **Fig 4. Confirmation of “Metal gel-shift” mechanism.**

488 A. Effect of EDTA and Ni²⁺ ion treatment on migration rate of recombinant Hpn in SDS-
489 PAGE (polyacrylamide-gel 20%). Lane M, protein marker; lane 1 and 2, Hpn before and after
490 boiling (3 min at 100°C), respectively; lanes 3 and 4, EDTA-treated Hpn without and with
491 boiling, respectively; lanes 5 and 6, Ni²⁺-treated Hpn without and with boiling, respectively.

492 B. The SDS-PAGE analysis of partially-metalated-Hpn (25 μM) treated with increasing
493 concentration of Ni²⁺ (1:0, 1:0.8, 1:1.2, 1:1.6, 1:2.0, 1:2.4, 1:2.8, 1:3.2, 1:3.6, 1:4.0, 1:6.0 and
494 1:8.0). Equal volume of heat-denatured protein applied in each lane.

495 C. Scheme used for MALDI-TOF-MS analysis of Hpn protein that was heat denatured in
496 Laemmli buffer. MS data was measured for Hpn treated with or without Ni²⁺ ion (1:6 mol
497 equivalent ratios). Further, MS data for Hpn (with or without Ni²⁺) treated in Laemmli buffer
498 (before and after SDS-PAGE) was measured. Even though some interference due to adducts
499 was observed in samples treated with Laemmli buffer or gel-eluted fractions, metalated peaks
500 (showing Hpn-Ni²⁺ complexes) were distinct. The occurrence of metalated peaks was
501 observed only for Ni²⁺-treated Hpn in all the conditions.

502

503 Moreover, EDTA-treated Hpn showed only one band of ~7 kDa on 20%
504 polyacrylamide-gel. On the other hand, the only protein band observed in Ni²⁺-treated Hpn
505 was of compact lower-size <7 kDa. Appearance of only one of the either band demonstrates
506 that both bands were derived from same protein i.e. Hpn. The partially-metalated Hpn treated
507 with relatively lower mol equivalent proportion of Ni²⁺ (0.0, 0.8, 1.2, 1.6, 2.0, 2.4, 2.8, 3.2,
508 3.6, 4.0, 6.0 and 8.0) demonstrated gradual shift with decrease in homogeneity of upper band
509 followed by increased intensity of compact lower band (**Fig4B**).

510 The Hpn protein treated for SDS-PAGE analyses was directly used for MALDI-TOF-
511 MS measurements and mass spectra of Ni²⁺-treated Hpn only showed peaks for protein-metal
512 complexes (**Fig 4C**). The mass spectra of protein fractions eluted from SDS-gel
513 corresponding to ~7 kDa and compact <7 kDa on 20% gel were measured. Only lower
514 compact band (<7 kDa) confirmed mass spectra for partially preserved protein-metal
515 complexes (**Fig 4C**). This MS data prompted us to quantify the metal-content of SDS-gel-

516 eluted bands. The Ni²⁺ content in lower compact bands (combining several gel slices
517 together) was detectable in ICP-OES. Measurements for EDTA-treated Hpn band were below
518 the detection limit signifying no metal bound to Hpn protein.

519 Several studies have reported preservation of protein-metal complex in SDS-PAGE
520 (**supporting information, S2 Table in S1 file**) and also in MALDI technique (**Table 3**). Thus,
521 those studies have provided experimental evidence that some metal-binding
522 proteins/metalloproteins can retain protein-metal complex even after using “harsh”
523 experimental protocols (i.e. use of SDS, denaturing agents, acidic matrices, organic solvents
524 or heating). Therefore, it is postulated that the methodology employed in the present study
525 was able to detect Hpn-Ni²⁺ complex and it was not a consequence of artifact formation.
526 Previous circular dichroism (CD) studies have reported more compact structure (an increase
527 in β -sheet with reduced α -helical content) after Ni²⁺ binding to Hpn [5,6].

528 Taken together, these data indicate that preserved protein-metal complex forms a
529 more compact structure leading to faster migration on SDS-PAGE. This phenomenon of
530 reversible shift in position when treated with either EDTA or Ni²⁺ was termed as “metal gel-
531 shift”.

532 **Polyacrylamide-gel concentration determines migration rate of** 533 **Hpn on SDS-PAGE regardless of “metal gel-shift”**

534 Polyacrylamide-gel concentration can dictate the migration speed of some
535 polypeptides [31]. To test the hypothesis that “metal gel-shift” is related to only Ni²⁺ binding
536 to Hpn or whether gel percentage has an effect on it, we thoroughly analyzed gel mobility of
537 apo-Hpn and Ni²⁺-treated Hpn with different polyacrylamide-gel concentrations. This concept
538 was investigated with purified Hpn after removing trace amounts of Ni²⁺ (**Fig 5A**). The
539 migration distance of apo-Hpn and Ni²⁺-treated Hpn relative to marker proteins (Nacalai
540 Tesque, Inc. Japan) was analyzed using ImageJ software [52] (**protocol provided in**

541 **Supporting information, Annexure A in S1 file).** Outcomes from these experiments were in
542 agreement with our hypothesis; the Ni²⁺-treated Hpn migrated faster than untreated Hpn
543 showing MW difference of 3-4 kDa (**Fig 5B**). These results demonstrated that apo-Hpn
544 migrated slowly in contrast to Ni²⁺-treated Hpn in all analyzed polyacrylamide-gel
545 concentrations, signifying that “metal gel-shift” is intimately associated with Ni²⁺-binding to
546 Hpn. This also shows that higher polyacrylamide-gel concentrations resulted in faster
547 migration of both the forms on SDS-PAGE (with and without Ni²⁺).

548

549 **Fig 5. Effect of polyacrylamide-gel concentration on migration speed of recombinant**
550 **Hpn without or with metal-treatment on SDS-PAGE.**

551 A. Relative position of apo- and Ni²⁺-treated Hpn protein depending on the polyacrylamide
552 percentage (15, 18, 20 and 22.5%) in gels. The SDS-gel electrophoresis was done till
553 bromophenol blue dye reached to the bottom in all gels. Therefore, theoretical MW values for
554 marker proteins- lysozyme (14.4 kDa) and Trypsin inhibitor (21.5 kDa) were taken into
555 consideration for estimation of apparent MW using ImageJ software (protocol provided in
556 Supplementary information as Annexure A). Red dotted line depicts expected position
557 corresponding to theoretical MW (~6.9 kDa).

558 B. The apparent MW of apo- and Ni²⁺-treated Hpn separated on different polyacrylamide-gel
559 concentrations was estimated by comparing relative migration distance of Hpn with globular
560 marker proteins on SDS-PAGE.

561

562 **Analysis of non-covalent Hpn-Ni²⁺ complexes**

563 We evaluated inter-conversion of Hpn-metal complexes using purified Hpn by
564 MALDI-TOF-MS. Although non-covalent complexes are expected to be stable at
565 physiological pH, acidic conditions or organic solvents used in matrix preparation may not be
566 the only factors important in the dissociation and prevent detection of these complexes in
567 MALDI analysis [53]. In this work, we applied full-length Hpn protein for studying Ni²⁺
568 binding. First, we standardized the set of conditions for acquisition of spectra for intact Hpn,

569 and then we investigated different types of matrices to analyze protein-metal ion complexes.
570 Among the tested combinations of acidic and non-acidic matrices, we found a mildly acidic
571 matrix (100% ACN, 0.01% TFA, and distilled water; v:v, 50:10:40) was most suitable in our
572 experimental conditions, and this was used in subsequent spectral measurements. This is the
573 first study reporting the successful application of MALDI-TOF-MS for investigating protein-
574 Ni²⁺ ion complexes. The MS data showed the progressive appearance of all possible metal-
575 bound species of Hpn, signifying that binding of metal ions at each site on protein may occur
576 independently. Moreover, a decrease in spectral intensity of the apo-protein with increasing
577 amounts of Ni²⁺ and increased intensity of metalated species provided conclusive evidence
578 for the binding of Ni²⁺ to Hpn.

579 To evaluate Ni²⁺ binding, Hpn treated with increasing molar concentrations of NiSO₄
580 solution was analyzed. Generally, the peaks of protein-metal complexes are smaller than the
581 peak of the apo-protein, even if a protein-metal interaction is already known to exist.
582 Therefore, higher amounts of Ni²⁺ were added to Hpn after confirming that no obstruction
583 was caused by it in the MALDI spectrum. Ni²⁺ solution was added to apo-Hpn (25 μM), pH
584 7.5 at an increasing mol equivalent ratio of Hpn to Ni²⁺ ion. After 1 h incubation at room
585 temperature, protein-metal solution was mixed with matrix and MS were acquired as
586 described above (**Fig 6**).

587

588 **Fig 6. MALDI-TOF-MS analysis of Ni²⁺ binding to Hpn.**

589 A. Spectra obtained with increasing concentrations of Ni²⁺ (1:0, 1:1, 1:2.5, 1:5, 1:10, 1:20
590 and 1:40, mol equivalent from top to bottom, respectively) added to apo-Hpn (25 μM) shown
591 in the right panel, and enlarged view of three representative spectra (1:0, 1:10 and 1:40)
592 shown with molecular mass of each peak in the left side. Numbers above dotted line
593 correspond to the number of Ni²⁺ bound to Hpn protein.

594 B. Mass difference calculated between adjacent peaks was found to be approximately equal
595 to the molecular mass of the Ni²⁺ ion (58.69) with the loss of two H⁺ atoms (molecular

596 weight [MW] of $H^+ = 1.00794$) upon metal binding.

597 C. Model of Ni^{2+} ion binding to Hpn. Order of occurrence has drawn on the basis of peak
598 intensity obtained in MALDI-TOF-MS data.

599

600 Representative MS of metalated species of Hpn clearly detected a progression with
601 seven major peaks (at m/z 6937.66, 6993.06, 7049.55, 7105.76, 7162.59, 7218.94, and
602 7275.33). The MS showed peaks of diverse intensity ranging from two to six Ni^{2+} ions bound
603 to Hpn (**Fig 6A**), with no specific species dominant in all the measured protein to metal ratios.
604 The mass differences between adjacent peaks were about m/z 56.7 (**Fig 6B**), matching the
605 added Ni^{2+} ion (m/z 58.69 of Ni^{2+}) with the loss of two hydrogen residues during the
606 ionization (m/z 1.007825×2). Overlay analysis of MS with and without Ni^{2+} showed slight
607 mass differences (m/z) between expected and observed molecular masses may be due to
608 tightly bound ions as previously observed for UreE protein from *H. pylori* [54]. The seventh
609 and subsequent peaks were bifurcated possibly because of matrix adducts interference and
610 hence considered not reliable for assignment to Hpn- Ni^{2+} ion complex. Titration of Hpn with
611 relatively lower Ni^{2+} concentrations (1:5) indicated at least one preferential higher-affinity
612 site, peak intensities of the protein-metal complexes were not according to the loading
613 number of Ni^{2+} ions on binding sites of Hpn (1>0>2>5>4>3). Furthermore, a difference in
614 peak intensity with higher amounts of Ni^{2+} (1:40) was observed (3>4>2>5>6>1) suggesting
615 the presence of several binding sites with different affinity. The progressive appearance of
616 peaks for all of the possible Hpn- Ni^{2+} ion complexes implied that Ni^{2+} binding to Hpn
617 occurred in a non-cooperative way (**Fig 6C**) as reported in cysteine-rich human
618 metallothionein 1a [55] and histidine-rich *E. coli* SlyD protein [21].

619 **Ni^{2+} tolerance and accumulation in Hpn-expressing *E. coli* cells**

620 If there is higher metal accumulation inside cells expressing the recombinant metal-
621 binding protein, then it should show better cell growth with higher tolerance compare with

622 wild-type upon addition of higher amounts of metal to the culture. However, this
623 phenomenon was not observed in the current as well as previous studies in Hpn-producing *E.*
624 *coli* cells (Hpn+) compared with wild-type (Hpn-) grown in LB medium [5]. Even though
625 Hpn have more efficient metal-binding ability as observed in MALDI-TOF-MS analysis,
626 higher Ni²⁺ accumulation measured by ICP-OES (6× for Hpn+ compared with Hpn-) was not
627 correlated with higher tolerance and cell survival (<twice in Hpn+ compared with Hpn-) (**Fig**
628 **7A-C**). We hypothesized that an unknown composition of nutrients in LB medium may
629 compensate for toxicity or availability of free Ni²⁺ ion to cells. Therefore, we tested M9
630 medium with a defined nutrient composition. As shown in **Fig 7D-E**, there was almost no
631 further growth of wild-type (Hpn-) at 50 μM and 100 μM Ni²⁺ supplied in M9 medium but
632 Hpn producing cells (Hpn+) were grown normally with approximately 30 and 45 times
633 higher intracellular Ni²⁺ content respectively (**Fig 7F**).

634

635 **Fig 7. Ni²⁺ tolerance, cell survival, and accumulation in Hpn-expressing *E. coli*.**

636 Effect of Ni²⁺ on growth of *E. coli* in Luria-Bertani (LB) (panel A) and M9 medium (panel D).
637 Growth curve was plotted in terms of optical density (OD) against amount of Ni²⁺ added to
638 culture. Cell survival under Ni²⁺ stress analyzed by dots blot as shown in panel B (LB) and E
639 (M9). Panel C (LB) and F (M9) represent the intracellular Ni²⁺ content in *E. coli* expressing
640 *hpn* gene compare to that of without *hpn* gene.

641

642

643

644

645

646 Discussion and Conclusions

647 The main findings of current work are as follows: 1) Hpn forms multimers in native
648 state as well as SDS-resistant multimer when eluted with 400 mM imidazole in buffer; 2)
649 Ni²⁺-binding to Hpn altered antibody binding in western blot and ELISA signifying
650 differential exposure of His-rich region upon metal-binding; 3) higher polyacrylamide-gel
651 concentrations resulted in faster migration of Hpn in SDS-PAGE; 4) average molecular mass
652 of Hpn determined as m/z 6945.66±0.34; 5) Hpn forms SDS-resistant (preserved) protein-
653 metal complexes and exhibits metal-triggered shift in electrophoretic mobility causing “metal
654 gel-shift” mechanism; 6) MALDI-TOF-MS was effectively employed to study non-covalent
655 Hpn-Ni²⁺ ion complexes showing up to six Ni²⁺ ions bound per monomer in a non-
656 cooperative way suggesting an equilibrium between Hpn-metalated species dependent on
657 metal availability. These findings explore various unusual physicochemical aspects of Hpn.
658 Also, higher tolerance and Ni²⁺ accumulation in Hpn-expressing *Escherichia coli* than wild-
659 type in minimal (M9) and nutrient-rich (LB) supply suggests protective role and potential to
660 load higher amounts of Ni²⁺ that corroborating with MALDI-TOF-MS data.

661 The Hpn protein contains remarkably high number of histidine residues, mostly in
662 clusters (**Fig 1A**). Histidine is unique in its molecular structure with an imidazole ring in its
663 side chain (an aromatic motif), and this can act as a ligand for metallic cations and as a
664 hydrogen bond donor or acceptor. “Stacking” behavior of the aromatic rings of histidine can
665 be one possible mechanism responsible for the formation of non-covalent multimeric
666 complexes; however, this concept is yet to be understood clearly in multimeric proteins [56].
667 Elution buffer containing imidazole (400 μM) led to formation of SDS-resistant multimer that
668 survived even in reduction and heat denaturation but converted to apparent monomer in
669 denatured Ni²⁺-treated Hpn (**Fig 5**). The preserved SDS-resistant protein-protein oligomer is

670 reported for several proteins under certain chemical environment (**Supporting information,**
671 **S1 Table in S1 file**) [57–62].

672 **Gel shifting**

673 Protein migration can be affected by several factors including molecular size, shape,
674 net charge, MW of the protein, and polyacrylamide concentration [31]. SDS normally binds
675 at hydrophobic sites, therefore it is reasonable that denatured apo-Hpn migrates at a slower
676 rate compared with marker proteins, because of the higher amount of hydrophilic residues
677 and only one hydrophobic amino acid in the Hpn [23,25,28]. A smaller protein with a higher
678 number of hydrophilic residues may have a greater hydrodynamic radius than a larger protein
679 but weaker hydration [63]. Similar results are reported for cystic fibrosis transmembrane
680 conductance regulator for the reason that of a change in helical structure altered SDS-binding
681 indicating protein-SDS complex size was a more important factor than net charge [23] and its
682 interaction with the sieving effects of a polyacrylamide gel [25].

683 The SDS-PAGE data demonstrated that the polyacrylamide-gel concentration affects
684 the migration rate of Hpn. Similar results are observed in “gel shifting” patterns for
685 transmembrane proteins in SDS-PAGE [31]. This indicate as any factor that changes effective
686 molecular size and net charge of protein-SDS complex can affect migration speed depending
687 on polyacrylamide-gel concentration, specifically affecting its interaction with the available
688 space in SDS-gel matrix [23,24,31]. In case of Hpn, impact of “stacking” behavior seems to
689 exceed all other factors and may control the migration speed depending on polyacrylamide-
690 gel concentration. Taken together, interplay between protein-protein interaction and sieving
691 effects of gel matrix may be a significant factor that influences gel mobility.

692 **Metal gel-shift**

693 Generally, non-covalent interactions should disrupt during SDS-PAGE owing to
694 activity of SDS and reducing agent [60]. However, preservation of protein-metal complex in

695 SDS-PAGE is reported in several cases, possibly due to incomplete or “reconstructive
696 denaturation” (**Supporting information, S2 Table in S1 file**) [35,36,60,62,64–69].
697 Preservation of partial Hpn-Ni²⁺ complex even after electrophoretic separation implies
698 significant strength and stability of Hpn-Ni²⁺ bond. Although exact mechanism of resistance
699 to reduction or denaturation and retaining metal ion is not yet known, similar results were
700 observed in case of platinum-binding proteins [70].

701 The change in electrophoretic mobility on SDS-PAGE after metal-binding to a protein
702 is rarely acknowledged except for some Ca²⁺-binding proteins including calmodulin isoforms
703 [36,37]. The wild-type and recombinant CDPKs from soybean [38], tobacco [39] and
704 Arabidopsis [40] display shift in electrophoretic mobility on SDS-PAGE and migrate faster or
705 slower depending on Ca²⁺ availability and is probably due to Ca²⁺-induced conformational
706 change [40]. The protein band of apo-Hpn was not as sharp as that of Ni²⁺-treated Hpn, which
707 might be caused by conformational changes upon metal binding. Thus, higher degree of
708 compactness or somehow altered SDS-binding to protein-metal complex that may allow
709 faster migration of Ni²⁺-treated Hpn than apo-Hpn. Faster migration on SDS-PAGE of
710 unreduced against reduced lysozyme [71] and for a membrane protein OmpA [72] also
711 suggested a possible role of structural compactness in “gel shifting”. Considering added MW
712 of metal ions, theoretical MW of Hpn protein in “metal-gel shift” band is higher than apo-
713 Hpn band. On the contrary, “metal-gel shift” band is migrating faster to lower position
714 compared to apo-Hpn band indicating conformational change (and not actual MW) is
715 decisive in governing migration rate.

716 From the experimental results, mechanism of “gel shifting” and “metal gel-shift” can
717 be described as shown in **Fig 8**. Anomalous migration of apo-Hpn (scheme highlighted with
718 yellow background) or metal-bound Hpn (scheme highlighted with green background) might
719 be due to differential amounts of SDS bound to protein, histidine stacking, altered

720 hydrodynamic radius, degree of compactness after metal-binding, or a combination of either
721 of these factors. The different structures are illustrated and discussed thoroughly in **Fig 8**.
722 Nevertheless, there might be additional biochemical and biophysical processes governing
723 differential protein migration in SDS-PAGE that is not explained in this scheme.

724

725 **Fig 8. Probable interrelationship between differential electrophoretic mobility of Hpn**
726 **and Ni²⁺ binding.**

727 Hpn may not have a definite form in the absence of Ni²⁺ (A). After denaturation (B), smaller
728 amounts of SDS binding/stacking behavior/larger hydrodynamic radius as well as a
729 combination of some or all of these conditions (C) might have resulted in slower migration
730 on SDS-PAGE (scheme highlighted with yellow background). Ni²⁺-treated Hpn forms a more
731 compact structure (D). Pictorial structure of metalated Hpn is drawn to explain the model.
732 MALDI spectra showed a partial Ni²⁺ bound form (E) in denatured SDS-PAGE. Altered
733 binding of SDS (F) caused by replacement of protein-protein to protein-SDS contacts
734 (inhibiting stacking behavior) and/or degree of compactness (or reduced hydrodynamic
735 radius) may be key factors responsible for “metal gel-shift” (scheme highlighted with green
736 background). β-ME, β-mercaptoethanol; EDTA, ethylene diaminetetraacetic acid.

737

738 The binding of non-denatured Hpn to Ni²⁺ column and reversible “metal-gel shift” in
739 SDS-PAGE presented herein together with previous CD studies [5] indicated that Hpn protein
740 could easily exchange metal ion suggesting the position of metal-binding domains are solvent
741 exposed and present at Hpn surface. Metal-induced structural changes leading to the
742 formation of a definite form has been reported for several other proteins, mostly associated
743 with β-turns [21,73]. Accordingly, metal-binding region (not entirely hidden inside the
744 structure of protein) could easily accessible for metal exchange and may involve small but
745 unique structural rearrangements.

746 **Metal gel-shift and MS data**

747 The pre-requisite for successful application of any mass spectrometry technique while

748 studying protein-metal interactions is the optimization of suitable method that preserves non-
 749 covalent complexes. The MALDI technique has been used previously to study non-covalent
 750 protein complexes (**Table 3**) by adjusting the range of parameters in order to preserve the
 751 non-covalent interactions during acquisition of spectra [46,47,90].

752

753 **Table 3. List of non-covalent protein-metal ion interactions studied by MALDI in**
 754 **combination with other methods.**

Peptide	Metal	Matrix solution	Combined method	Reference
(GHHPH) ₅ G peptide	Cu	DHB	TOF-MS	[74]
Human glycoprotein	Cu	DHB in 0.1% aqueous TFA	TOF-MS	[75]
Zinc finger peptides	Zn	HCCA in 1:1 ammonium bicarbonate (1M)-ethanol.	-	[76]
Prion protein	Cu	DHB and 6,7-dihydroxycoumarin	TOF-MS	[77]
Ferrichrome	Fe	DHB in methanol	TOF-MS	[78]
Luteinizing hormone releasing hormone	Ni, Cu, Zn	Paranitroaniline in ethanol (10 mg/mL)	Fourier Transform-MS	[79]
Zinc finger peptide	Zn	6-aza-2-thiothymine or DHB in Tris (10 mM), ammonium bicarbonate (20 mM) or 0.1% TFA	TOF-MS	[80]
Bradykinin	Cu, Ag, Co, Ni, Zn	HCCA matrix saturated in water and acetonitrile (70:30 v/v) containing 0.1% TFA.	TOF-MS	[81]
Prion proteins	Cu	Sinapinic acid in 20% acetonitrile	TOF-MS	[82]
Human brain proteins	Cu, Zn	DHB in acetonitrile and 0.1% TFA in water (2:1)	FT-ICR -MS	[83]

Human tau proteins	Cu, Zn	DHB in acetonitrile and 0.1% TFA in water (2:1)	FT-ICR -MS	[84]
Human brain proteins	P, Cu, Zn, Fe	DHB in acetonitrile: 0.1% TFA in water (2:1)	FT-ICR-MS	[85]
Angiotensin I	Cu, K	HCCA, 3-aminoquinoline and glycerol	TOF-MS	[86]
Rat tissues	Zn, Cu, Fe, Cr, Cd, Pb	HCCA in acetonitrile:0.1% TFA in water (2:1)	TOF-MS and LA-ICP-MS	[87]
a-Crystallin	Zn	HCCA in 1:2 acetonitrile and 0.1 % TFA	TOF-MS	[88]
Protein fraction from Brazil nuts	Cu	HCCA in 50% acetonitrile and 0.1% TFA	TOF-MS	[89]
Hpn	Ni	Sinapinic acid (100% ACN, 0.01% TFA, and distilled water; v:v, 50:10:40)	TOF-MS	Present study

755 (DHB: 2,5-dihydroxybenzoic acid; HCCA: α -cyano-4-hydroxycinnamic acid; FT-ICR-MS:
 756 Fourier transform-ion cyclotron resonance-mass spectrometry; LA-ICP-MS: Laser ablation-
 757 inductively coupled plasma-mass spectrometry)
 758

759 Using mild-acidic matrix, spectral measurements showed distinct peaks, validating
 760 one apo-Hpn peak with six of Hpn-Ni²⁺ complexes. Singly charged species of Hpn in
 761 MALDI-TOF-MS might allow detection of a sixth Hpn-Ni²⁺ complex in mild-acidic
 762 conditions that not reported in previous studies [6,7]. However, appearance of weaker or non-
 763 specific protein-metal complexes due to higher amounts of metal added to protein samples is
 764 a limitation of the ionization process in positive mode measurements [21] and this possibility
 765 for sixth Hpn-Ni²⁺ complex cannot be excluded. The interfaces of metal ions with histidine-
 766 rich peptides have not been investigated so far, perhaps because such peptides are not
 767 possible to study with routinely used techniques owing to overlapping signals [91]. Even
 768 though MS data alone are not sufficient to interpret the exact mechanism of metal-binding to
 769 various sites, these data have revealed the high flexibility (plasticity) of Hpn for Ni²⁺ binding
 770 and its potential to load higher amounts of Ni²⁺ in such a small structure of ~7 kDa.

771 Our MS data imply several key points that are complementary to “metal gel-shift”. At
772 first, all available Hpn molecules were in metalated form at higher Ni²⁺ in MS data. Similarly,
773 presence of only “metal-gel shift” band at higher Ni²⁺ was observed on SDS-PAGE (**Fig 4B**).
774 Second, Hpn showed MS peaks for metalated species even treated with lower metal
775 concentrations (**Fig 6**). This coincides with the appearance of "metal-gel shift" band in all
776 protein-metal molar ratios (lower to higher) on SDS-PAGE (**Fig 4B and C**). Third, mass
777 spectral intensity for apo-Hpn gradually decreased in Ni²⁺-treated Hpn and subsequently mass
778 spectral intensity for either of the metalated species was increased in respective
779 measurements showing progressive appearance of Hpn-Ni²⁺ peaks. This is also consistent
780 with the gradual increase in heterogeneity of apo-Hpn band followed by compact "metal-gel
781 shift" band.

782 Interestingly, at relatively higher amount of Ni²⁺, distribution of mass for each Hpn-
783 Ni²⁺ complex was highly heterogeneous in MS data but on contrary, SDS-PAGE showed only
784 one compact protein band. Electrophoretic separation of metalated species having smaller
785 mass difference of each added Ni²⁺ (0.055 kDa) cannot be distinguished on regular SDS-
786 PAGE owing to limited resolution. Also, several factors can affect the migration of each
787 metalated species of Hpn on SDS-PAGE including consequence of boiling, Laemmli buffer
788 components, re-arrangement of protein-protein, protein-metal, and/or protein-SDS
789 interactions. But this is not the case in MS measurements. Moreover, previous studies
790 suggested involvement of almost all the four cysteine residues in Ni²⁺-binding [5,10–12].
791 Therefore, partial or complete reduction of disulfide bonds in two pairs of cysteine residues
792 may release some but not all metal ions bound to Hpn during “constructive” denaturation. It
793 may produce partially-metalated Hpn species in equilibrium (observed in MS of protein
794 fractions before and after SDS-PAGE, **Fig 4C**) that migrated as homogenous “metal gel-shift”
795 band on SDS-PAGE. In addition, differential ionization efficiency and ion suppression effect

796 in MS may interfere in mass-to-charge ratio [92]. The thermodynamic structures of the apo-
797 protein for metalation and the fully metalated protein for demetalation may not be the same
798 [21]. Thus, without further structural studies, it is intricate to compare precise mass
799 distribution of metalated species on SDS-PAGE and further studies are under investigation.
800 Nevertheless, “metal-gel shift” together with MALDI-TOF-MS data establishes that the
801 positional shift is directly associated with metal-binding to Hpn and it is reversible upon
802 metal removal.

803 In brief, our study reveals a novel mechanism of “metal gel-shift” responsible for
804 shifts in electrophoretic gel mobility of Ni²⁺-treated Hpn on SDS-PAGE signifying metal-
805 induced conformational changes. This property can be used to explore interactions between
806 histidine-rich proteins and surfactant to investigate how metal-binding to a histidine-rich
807 protein changes its confirmation and hydrophobic or electrostatic interactions.

808

809

810

811

812

813

814

815

816

817 **Conflict of interest**

818 The authors declare that they have no conflicts of interest with the contents of this article.

819 **Author contributions**

820 HH and EHM conceived the idea for the project, supervised the study, provided essential
821 reagents and edited the manuscript. RMS conducted most of the experiments, analyzed the
822 results and wrote the manuscript. YI and JM conducted *H. pylori* culture experiments
823 including genome DNA extraction and gene cloning. All authors edited the manuscript,
824 reviewed the results and approved the final draft of this manuscript.

825 **Acknowledgement**

826 The protocol and facility to perform ELISA was kindly provided by Dr. T. Tsuboi and Dr. E.
827 Takashima (Division of Malaria Research, Proteo-Science Center, Ehime University,
828 Matsuyama, Ehime, Japan).

829

830

831

832

833

834

835

836

837

838

839

840

841 **References**

- 842 1. Cheng T, Xia W, Wang P, Huang F, Wang J, Sun H. Histidine-rich proteins in
843 prokaryotes: metal homeostasis and environmental habitat-related occurrence.
844 *Metallomics*. 2013; 5: 1423. doi:10.1039/c3mt00059a
- 845 2. Koonin EV, Wolf YI. Genomics of bacteria and archaea: the emerging dynamic view
846 of the prokaryotic world. *Nucleic Acids Res*. 2008; 36: 6688–6719.
847 doi:10.1093/nar/gkn668
- 848 3. de Reuse H, Vinella D, Cavazza C. Common themes and unique proteins for the
849 uptake and trafficking of nickel, a metal essential for the virulence of *Helicobacter*
850 *pylori*. *Front Cell Infect Microbiol*. 2013; 3: 1–6. doi:10.3389/fcimb.2013.00094
- 851 4. Gilbert JV, Ramakrishna J, Sunderman FW, Wright A, Plaut AG. Protein Hpn \square :
852 Cloning and characterization of a histidine-rich metal-binding polypeptide in
853 *Helicobacter pylori* and *Helicobacter mustelae*. 1995; 63: 2682–2688.
- 854 5. Ge R, Watt RM, Sun X, Tanner J a, He Q-Y, Huang J-D, et al. Expression and
855 characterization of a histidine-rich protein, Hpn: potential for Ni²⁺ storage in
856 *Helicobacter pylori*. *Biochem J*. 2006; 393: 285–93. doi:10.1042/BJ20051160
- 857 6. Ge R, Zhang Y, Sun X, Watt RM, He Q-Y, Huang J-D, et al. Thermodynamic and
858 kinetic aspects of metal binding to the histidine-rich protein, Hpn. *J Am Chem Soc*.
859 2006; 128: 11330–1. doi:10.1021/ja062589t
- 860 7. Wegner SV, Ertem E, Sunbul M, He C. Metal-binding properties of Hpn from
861 *Helicobacter pylori* and implications for the therapeutic activity of bismuth. *Chem Sci*.
862 2011; 2: 451. doi:10.1039/c0sc00411a
- 863 8. Mobley HL, Garner RM, Chippendale GR, Gilbert JV, Kane AV, Plaut AG. Role of
864 Hpn and NixA of *Helicobacter pylori* in susceptibility and resistance to bismuth and
865 other metal ions. *Helicobacter*. 1999; 4: 162–169. PMID: 10469190

- 866 9. Seshadri S, Benoit SL, Maier RJ. Roles of His-rich Hpn and Hpn-like proteins in
867 *Helicobacter pylori* nickel physiology. *J Bacteriol.* 2007; 189: 4120–6.
868 doi:10.1128/JB.01245-06
- 869 10. Witkowska D, Politano R, Rowinska-Zyrek M, Guerrini R, Remelli M, Kozlowski H.
870 The coordination of NiII and CuII ions to the polyhistidyl motif of Hpn protein: Is it
871 as strong as we think? *Chem - A Eur J.* 2012; 18: 11088–11099.
872 doi:10.1002/chem.201200780
- 873 11. Chiera NM, Rowinska-Zyrek M, Wiczorek R, Guerrini R, Witkowska D, Remelli M,
874 et al. Unexpected impact of the number of glutamine residues on metal complex
875 stability. *Metallomics.* 2013; 5: 214–21. doi:10.1039/c3mt20166j
- 876 12. Rowinska-Zyrek M, Witkowska D, Bielinska S, Kamysz W, Kozlowski H. The -Cys-
877 Cys- motif in *Helicobacter pylori*'s Hpn and HspA proteins is an essential anchoring
878 site for metal ions. *Dalton Trans.* 2011; 40: 5604–10. doi:10.1039/c1dt10187k
- 879 13. Vinella D, Fischer F, Vorontsov E, Gallaud J, Malosse C, Michel V, et al. Evolution of
880 *Helicobacter*: Acquisition by gastric species of two histidine-rich proteins essential for
881 colonization. *PLoS Pathog.* 2015; 11: 1–32. doi:10.1371/journal.ppat.1005312
- 882 14. Zhou Q, Qi S, Sun X, Ge R. The interaction of a histidine-rich protein hpn with the
883 membrane mimics: implications for pathologic roles of Hpn in *Helicobacter pylori*.
884 *Helicobacter.* 2014; 19: 129–35. doi:10.1111/hel.12109
- 885 15. Zeng YB, Zhang DM, Li H, Sun H. Binding of Ni²⁺ to a histidine- and glutamine-
886 rich protein, Hpn-like. *J Biol Inorg Chem.* 2008; 13: 1121–1131. doi:10.1007/s00775-
887 008-0397-0
- 888 16. Brayman TG, Hausinger RP. Purification, characterization, and functional analysis of
889 a truncated *Klebsiella aerogenes* UreE urease accessory protein lacking the histidine-
890 rich carboxyl terminus. *J Bacteriol.* 1996; 178: 5410–6. PMID: PMC178359

- 891 17. Chan K-H, Li T, Wong C-O, Wong K-B. Structural Basis for GTP-dependent
892 dimerization of hydrogenase maturation factor HypB. *PLoS One*. 2012; 7: e30547.
893 doi:10.1371/journal.pone.0030547
- 894 18. Fu C, Olson JW, Maier RJ. HypB protein of *Bradyrhizobium japonicum* is a metal-
895 binding GTPase capable of binding 18 divalent nickel ions per dimer. *Proc Natl Acad*
896 *Sci U S A*. 1995; 92: 2333–2337. doi:10.1073/pnas.92.6.2333
- 897 19. Rey L, Imperial J, Palacios JM, Ruiz-Argüeso T. Purification of *Rhizobium*
898 *leguminosarum* HypB, a nickel-binding protein required for hydrogenase synthesis. *J*
899 *Bacteriol*. 1994; 176: 6066–6073. PMID: 7928968
- 900 20. Hottenrott S, Schumann T, Plückthun a, Fischer G, Rahfeld JU. The *Escherichia coli*
901 SlyD is a metal ion-regulated peptidyl-prolyl cis/trans-isomerase. *J Biol Chem*. 1997;
902 272: 15697–701. doi:10.1074/jbc.272.25.15697
- 903 21. Kaluarachchi H, Sutherland DE, Young A, Pickering IJ, Stillman MJ, Zamble DB.
904 The Ni(II)-binding properties of the metallochaperone SlyD. *J Am Chem Soc*. 2009;
905 131: 18489–18500. doi:10.1021/ja9081765
- 906 22. Jeon WB, Cheng J, Ludden PW. Purification and characterization of membrane-
907 associated CooC protein and its functional role in the insertion of nickel into carbon
908 monoxide dehydrogenase from *Rhodospirillum rubrum*. *J Biol Chem*. 2001; 276:
909 38602–38609. doi:10.1074/jbc.
- 910 23. Rath A, Glibowicka M, Nadeau VG, Chen G, Deber CM. Detergent binding explains
911 anomalous SDS-PAGE migration of membrane proteins. *Proc Natl Acad Sci U S A*.
912 2009; 106: 1760–1765. doi:10.1073/pnas.0813167106
- 913 24. Shi Y, Mowery R a., Ashley J, Hentz M, Ramirez AJ, Bilgicer B, et al. Abnormal
914 SDS-PAGE migration of cytosolic proteins can identify domains and mechanisms that
915 control surfactant binding. *Protein Sci*. 2012; 21: 1197–1209. doi:10.1002/pro.2107

- 916 25. Tulumello DV, Deber CM. Positions of polar amino acids alter interactions between
917 transmembrane segments and detergents. *Biochemistry*. 2011; 50: 3928–3935.
918 doi:10.1021/bi200238g
- 919 26. Karch CM, Borchelt DR. Aggregation modulating elements in mutant human
920 superoxide dismutase 1. *Arch Biochem Biophys*. Elsevier Inc.; 2010;503: 175–82.
921 doi:10.1016/j.abb.2010.07.027
- 922 27. Cun S, Li H, Ge R, Lin MCM, Sun H. A Histidine-rich and Cysteine-rich Metal-
923 binding Domain at the C Terminus of Heat Shock Protein A from *Helicobacter pylori*:
924 Implication for nickel homeostasis and bismuth susceptibility. *J Biol Chem*. 2008;
925 283: 15142–15151. doi:10.1074/jbc.M800591200
- 926 28. Panayotatos N, Radziejewska E, Acheson A, Pearsall D, Thadani A, Wong V.
927 Exchange of a single amino acid interconverts the specific activity and gel mobility of
928 human and rat ciliary neurotrophic factors. *J Biol Chem*. 1993;268: 19000–3.
929 Pubmed: 8395524
- 930 29. Hayward LJ. Decreased metallation and activity in subsets of mutant superoxide
931 dismutases associated with familial amyotrophic lateral sclerosis. *J Biol Chem*. 2002;
932 277: 15923–15931. doi:10.1074/jbc.M112087200
- 933 30. Saha S, Biswas KH, Kondapalli C, Isloor N, Visweswariah SS. The Linker Region in
934 Receptor Guanylyl Cyclases Is a Key Regulatory Module: mutational analysis of
935 guanylyl cyclase C. *J Biol Chem*. 2009; 284: 27135–27145.
936 doi:10.1074/jbc.M109.020032
- 937 31. Rath A, Cunningham F, Deber CM. Acrylamide concentration determines the
938 direction and magnitude of helical membrane protein gel shifts. *Proc Natl Acad Sci U*
939 *S A*. 2013; 110: 15668–73. doi:10.1073/pnas.1311305110
- 940 32. Lee A, Rourke JO, Ungria MCDE, Robertson B, Daskalopoulos G, Dixon MF. A

- 941 standardized mouse model of *Helicobacter pylori* infection: introducing the Sydney
942 strain. 1997; 112: 1386–1397. PMID: 9098027
- 943 33. Raab A, Pioselli B, Munro C, Thomas-Oates J, Feldmann J. Evaluation of gel
944 electrophoresis conditions for the separation of metal-tagged proteins with subsequent
945 laser ablation ICP-MS detection. *Electrophoresis*. 2009; 30: 303–314.
946 doi:10.1002/elps.200800264
- 947 34. Sussulini A, Becker JS. Combination of PAGE and LA-ICP-MS as an analytical
948 workflow in metallomics: state of the art, new quantification strategies, advantages
949 and limitations. *Metallomics*. 2011;3: 1271. doi:10.1039/c1mt00116g
- 950 35. Otzen D. Protein-surfactant interactions: A tale of many states. *Biochim Biophys Acta*
951 - Proteins Proteomics; 2011; 1814: 562–591. doi:10.1016/j.bbapap.2011.03.003
- 952 36. Köhler C, Neuhaus G. Characterisation of calmodulin binding to cyclic nucleotide-
953 gated ion channels from *Arabidopsis thaliana*. *FEBS Lett*. 2000; 471: 133–136.
954 doi:10.1016/S0014-5793(00)01383-1
- 955 37. Damiani E, Margreth A. Subcellular fractionation to junctional sarcoplasmic
956 reticulum and biochemical characterization of 170 kDa Ca(2+)- and low-density-
957 lipoprotein-binding protein in rabbit skeletal muscle. *Biochem J*. 1991; 277: 825–832.
958 PMID: 1872815
- 959 38. Li J, Lee YJ, Assmann SM. Guard Cells Possess a Calcium-Dependent Protein Kinase
960 That Phosphorylates the KAT1 Potassium Channel 1. *Plant Physiol*. 1998; 116: 785–
961 795. PMID: 9489023
- 962 39. Yoon GM, Cho HS, Ha HJ, Liu JR, Lee HP. Characterization of NtCDPK1, a
963 calcium-dependent protein kinase gene in *Nicotiana tabacum*, and the activity of its
964 encoded protein. *Plant Mol Biol*. 1999; 39: 991–1001. PMID: 10344204
- 965 40. Romeis T, Franz S, Ehlert B, Liese A, Kurth J, Cazale A. Calcium-Dependent Protein

- 966 Kinase CPK21 Functions in Abiotic Stress Response in *Arabidopsis thaliana*. 2011; 4.
967 doi:10.1093/mp/ssq064
- 968 41. Akiyama H, Kanai S, Hirano M, Miyasaka H. A novel plasmid recombination
969 mechanism of the marine cyanobacterium *Synechococcus* sp. PCC7002. *DNA Res.*
970 1998; 5: 327–34. Pubmed: 10048481
- 971 42. Yamauchi S, Ueda Y, Matsumoto M, Inoue U, Hayashi H. Distinct features of protein
972 folding by the GroEL system from a psychrophilic bacterium, *Colwellia*
973 *psychrerythraea* 34H. *Extremophiles*. 2012; 16: 871–882. doi:10.1007/s00792-012-
974 0483-7
- 975 43. Laemmli UK. Cleavage of structural proteins during the assembly of the head of
976 bacteriophage T4. *Nature*; 1970. pp. 680–685. doi:10.1038/227680a0
- 977 44. Miura K, Orcutt AC, Muratova O V., Miller LH, Saul A, Long CA. Development and
978 characterization of a standardized ELISA including a reference serum on each plate to
979 detect antibodies induced by experimental malaria vaccines. *Vaccine*. 2008; 26: 193–
980 200. doi:10.1016/j.vaccine.2007.10.064
- 981 45. Jin Y, Manabe T. High-efficiency protein extraction from polyacrylamide gels for
982 molecular mass measurement by matrix-assisted laser desorption/ionization-time of
983 flight-mass spectrometry. *Electrophoresis*. 2005; 26: 1019–1028.
984 doi:10.1002/elps.200410187
- 985 46. Schlosser G, Pocsfalvi G, Malorni A, Puerta A, de Frutos M, Vekey K. Detection of
986 immune complexes by matrix-assisted laser desorption/ionization mass spectrometry.
987 *Rapid Commun Mass Spectrom*. 2003; 17: 2741–2747. doi:10.1002/rcm.1239
- 988 47. Rom S, Gilad A, Kalifa Y, Konrad Z, Karpasas MM, Goldgur Y, et al. Mapping the
989 DNA- and zinc-binding domains of ASR1 (abscisic acid stress ripening), an abiotic-
990 stress regulated plant specific protein. *Biochimie*. 2006; 88: 621–628.

- 991 doi:10.1016/j.biochi.2005.11.008
- 992 48. Mahadev SR, Hayashi H, Ikegami T, Abe S, Morita EH. Improved Protein
993 Overexpression and Purification Strategies for Structural Studies of Cyanobacterial
994 Metal-Responsive Transcription Factor, SmtB from Marine *Synechococcus* sp. PCC
995 7002. *Protein J.* 2013; 32: 626–634. doi:10.1007/s10930-013-9525-y
- 996 49. Watanabe Y, Aburatani K, Mizumura T, Sakai M, Muraoka S, Mamegosi S, et al.
997 Novel ELISA for the detection of raw and processed egg using extraction buffer
998 containing a surfactant and a reducing agent. *J Immunol Methods.* 2005; 300: 115–
999 123. doi:10.1016/j.jim.2005.02.014
- 1000 50. Lechtzier V, Hutoran M, Levy T, Kotler M, Brenner T, Steinitz M. Sodium dodecyl
1001 sulphate-treated proteins as ligands in ELISA. *J Immunol Methods.* 2002; 270: 19–26.
1002 doi:10.1016/S0022-1759(02)00214-4
- 1003 51. Burgess NK, Dao TP, Stanley AM, Fleming KG. β -Barrel Proteins That Reside in the
1004 *Escherichia coli* Outer Membrane in Vivo Demonstrate Varied Folding Behavior in
1005 Vitro. *J Biol Chem.* 2008; 283: 26748–26758. doi:10.1074/jbc.M802754200
- 1006 52. Abràmoff MD, Magalhães PJ, Ram SJ. Image processing with imageJ. *Biophotonics*
1007 *Int.* 2004; 11: 36–41. doi:10.1117/1.3589100
- 1008 53. Strupat K. Molecular Weight Determination of Peptides and Proteins by ESI and
1009 MALDI. 2005; 405: 1–36. doi:10.1016/S0076-6879(05)05001-9
- 1010 54. Shi R, Munger C, Asinas A, Benoit SL, Miller E, Matte A, et al. Crystal Structures of
1011 Apo and Metal-Bound Forms of the UreE Protein from *Helicobacter pylori*: Role of
1012 Multiple Metal Binding Sites,. *Biochemistry.* 2010; 49: 7080–7088.
1013 doi:10.1021/bi100372h
- 1014 55. Sutherland DEK, Stillman MJ. Noncooperative cadmium(II) binding to human
1015 metallothionein 1a. *Biochem Biophys Res Commun.* 2008; 372: 840–844.

- 1016 doi:10.1016/j.bbrc.2008.05.142
- 1017 56. Liao S-M, Du Q-S, Meng J-Z, Pang Z-W, Huang R-B. The multiple roles of histidine
1018 in protein interactions. *Chem Cent J*. 2013; 7: 44. doi:10.1186/1752-153X-7-44
- 1019 57. Kolodziejski PJ, Rashid MB, Eissa NT. Intracellular formation of “undisruptable”
1020 dimers of inducible nitric oxide synthase. *Proc Natl Acad Sci U S A*. 2003; 100:
1021 14263–8. doi:10.1073/pnas.2435290100
- 1022 58. Atwood CS, Scarpa RC, Huang X, Moir RD, Jones WD, Fairlie DP, et al.
1023 Characterization of copper interactions with Alzheimer amyloid β peptides:
1024 Identification of an attomolar-affinity copper binding site on amyloid β 1-42. *J*
1025 *Neurochem*. 2000; 75: 1219–1233. doi:10.1046/j.1471-4159.2000.0751219.x
- 1026 59. Tham SJ, Chang CD, Huang HJ, Lee YF, Huang TS, Chang CC. Biochemical
1027 characterization of an acid phosphatase from thermus thermophilus. *Biosci Biotechnol*
1028 *Biochem*. 2010;74: 727–735. doi:JST.JSTAGE/bbb/90773 [pii]
- 1029 60. Nowakowski AB, Wobig WJ, Petering DH. Native SDS-PAGE: high resolution
1030 electrophoretic separation of proteins with retention of native properties including
1031 bound metal ions. *Metallomics*. 2014;6: 1068–78. doi:10.1039/c4mt00033a
- 1032 61. Bullis BL, Li X, Rieder C V., Singh DN, Berthiaume LG, Fliegel L. Properties of the
1033 Na⁺/H⁺ exchanger protein detergent-resistant aggregation and membrane
1034 microdistribution. *Eur J Biochem*. 2002; 269: 4887–4895. doi:10.1046/j.1432-
1035 1033.2002.03202.x
- 1036 62. Pinato O, Musetti C, Farrell NP, Sissi C. Platinum-based drugs and proteins:
1037 Reactivity and relevance to DNA adduct formation. *J Inorg Biochem*. 2013;122: 27–
1038 37. doi:10.1016/j.jinorgbio.2013.01.007
- 1039 63. Erickson HP. Size and shape of protein molecules at the nanometer level determined
1040 by sedimentation, gel filtration, and electron microscopy. *Biol Proced Online*. 2009;

- 1041 11: 32–51. doi:10.1007/s12575-009-9008-x
- 1042 64. Solis C, Oliver A, Andrade E. PIXE analysis of proteins from a photochemical center.
1043 Nucl. Instr. Meth. Phys. Res. Sect. B, 1998; 136: 928–931. Available:
1044 <http://www.sciencedirect.com/science/article/pii/S0168583X97008963>
- 1045 65. Binet MRB, Ma R, McLeod CW, Poole RK. Detection and characterization of zinc-
1046 and cadmium-binding proteins in Escherichia coli by gel electrophoresis and laser
1047 ablation-inductively coupled plasma-mass spectrometry. Anal Biochem. 2003; 318:
1048 30–38. doi:10.1016/S0003-2697(03)00190-8
- 1049 66. Gao Y, Chen C, Zhang P, Chai Z, He W, Huang Y. Detection of metalloproteins in
1050 human liver cytosol by synchrotron radiation X-ray fluorescence after sodium dodecyl
1051 sulphate polyacrylamide gel electrophoresis. Anal Chim Acta. 2003; 485: 131–137.
1052 doi:10.1016/S0003-2670(03)00347-7
- 1053 67. Verbi FM, Arruda SCC, Rodriguez APM, Perez CA, Arruda MAZ. Metal-binding
1054 proteins scanning and determination by combining gel electrophoresis, synchrotron
1055 radiation X-ray fluorescence and atomic spectrometry. J Biochem Biophys Methods.
1056 2005; 62: 97–109. doi:10.1016/j.jbbm.2004.09.008
- 1057 68. Finney L, Chishti Y, Khare T, Giometti C, Levina A, Lay PA, et al. Imaging metals in
1058 proteins by combining electrophoresis with rapid X-ray fluorescence mapping. ACS
1059 Chem Biol. 2010; 5: 577–587. doi:10.1021/cb1000263
- 1060 69. Weseloh G, Kuhbacher M, Bertelsmann H, Ozaslan M, Kyriakopoulos A, Knochel A,
1061 et al. Analysis of metal-containing proteins by gel electrophoresis and synchrotron
1062 radiation X-ray fluorescence. J Radioanal Nucl Chem. 2004; 259: 473–477.
1063 doi:10.1023/B:JRNC.0000020921.66046.1c
- 1064 70. Mena ML, Moreno-Gordaliza E, Moraleja I, Canas B, Gomez-Gomez MM. OFFGEL
1065 isoelectric focusing and polyacrylamide gel electrophoresis separation of platinum-

- 1066 binding proteins. *J Chromatogr A*. 2011; 1218: 1281–1290.
1067 doi:10.1016/j.chroma.2010.12.115
- 1068 71. Pitt-Rivers R, Impiombato FS. The binding of sodium dodecyl sulphate to various
1069 proteins. *Biochem J*. 1968; 109: 825–830. PMID: PMC1187034
- 1070 72. Kleinschmidt JH, Wiener MC, Tamm LK. Outer membrane protein A of *E. coli* folds
1071 into detergent micelles, but not in the presence of monomeric detergent. *Protein Sci*.
1072 1999; 8: 2065–2071. doi:10.1110/ps.8.10.2065
- 1073 73. Chen SH, Chen L, Russell DH. Metal-induced conformational changes of human
1074 metallothionein-2A: A combined theoretical and experimental study of metal-free and
1075 partially metalated intermediates. *J Am Chem Soc*. 2014; 136: 9499–9508.
1076 doi:10.1021/ja5047878
- 1077 74. Hutchens TW, Nelson RW, Yip T. Evaluation of Peptide / Metal Ion Interactions by
1078 UV Laser Desorption Time-of-flight Mass Spectrometry. *J. Mol. Recogn*. 1991; 4:
1079 151–153. doi: 10.1002/jmr.300040407
- 1080 75. Nelson RW, Hutchens TW. Mass spectrometric analysis of a transition-metal-binding
1081 peptide using mass spectrometry. A demonstration of probe tip chemistry. *Rapid*
1082 *Commun Mass Spectrom* 1992; 6: 4–8. doi: 10.1002/rcm.1290060103
- 1083 76. Woods AS, Buchsbaum JC, Worrall TA, Berg JM, Cotter RJ. Matrix-Assisted Laser
1084 Desorption/Ionization of Noncovalently Bound Compounds. *Anal Chem*. 1995; 67:
1085 4462–4465. doi:10.1021/ac00120a005
- 1086 77. Hornshaw MP, McDermott JR, Candy JM. Copper binding to the N-terminal tandem
1087 repeat regions of mammalian and avian prion protein. *Biochem Biophys Res*
1088 *Commun*. 1995; 207: 621–629. doi:10.1006/bbrc.1995.1233
- 1089 78. Kaltashov IA, Cotter RJ, Harry W, Ketner GW. Ferrichrome: Surprising stability of a
1090 cyclic peptide-FeIII complex revealed by mass spectrometry. *J Am Soc Mass*

- 1091 Spectrom 1997; 8: 1070–1077. doi:10.1016/S1044-0305(97)00128-1
- 1092 79. Masselon C, Salih B, Zenobi R. Matrix-assisted laser desorption/ionization Fourier
1093 transform mass spectrometry of luteinizing hormone releasing hormone-metal ion
1094 complexes. *J Am Soc Mass Spectrom.* 1999; 10: 19–26. doi:10.1016/S1044-
1095 0305(98)00128-7
- 1096 80. Lehmann R, Zenobi R, Vetter S. Matrix-assisted laser desorption/ionization mass
1097 spectra reflect solution-phase zinc finger peptide complexation. *J Am Soc Mass*
1098 *Spectrom.* 1999; 10: 27–34. doi:10.1016/S1044-0305(98)00116-0
- 1099 81. Cerda BA, Cornett L, Wesdemiotis C. Probing the interaction of alkali and transition
1100 metal ions with bradykinin and its des-arginine derivatives via matrix-assisted laser
1101 desorption/ionization and postsorce decay mass spectrometry. *Int J Mass Spectrom.*
1102 1999; 193: 205–226. doi: 10.1016/S1387-3806(99)00164-5
- 1103 82. Qin K, Yang Y, Mastrangelo P, Westaway D. Mapping Cu(II) Binding Sites in Prion
1104 Proteins by Diethyl Pyrocarbonate Modification and Matrix-assisted Laser Desorption
1105 Ionization-Time of Flight (MALDI-TOF) Mass Spectrometric Footprinting. *J Biol*
1106 *Chem.* 2002; 277: 1981–1990. doi:10.1074/jbc.M108744200
- 1107 83. Becker JS, Zoriy M, Becker JS, Pickhardt C, Damoc E, Juhacz G, et al. Determination
1108 of phosphorus-, copper-, and zinc-containing human brain proteins by LA-ICPMS and
1109 MALDI-FTICR-MS. *Anal Chem.* 2005; 77: 5851–5860. doi:10.1021/ac0506579
- 1110 84. Becker JS, Zoriy M, Przybylski M, Becker JS. Study of formation of Cu- and Zn-
1111 containing tau protein using isotopically-enriched tracers by LA-ICP-MS and
1112 MALDI-FTICR-MS. *J Anal At Spectrom.* 2007; 22: 63–68. doi:10.1039/B609419H
- 1113 85. Becker JS, Zoriy M, Przybylski M, Becker JS. High resolution mass spectrometric
1114 brain proteomics by MALDI-FTICR-MS combined with determination of P, S, Cu, Zn
1115 and Fe by LA-ICP-MS. *Int J Mass Spectrom.* 2007; 261: 68–73.

- 1116 doi:10.1016/j.ijms.2006.07.016
- 1117 86. Hortal AR, Hurtado P, Martínez-Haya B. Matrix-assisted laser desorption mass
1118 spectrometry of gas-phase peptide–metal complexes. *Appl Phys A*. 2008; 93: 935–939.
1119 doi:10.1007/s00339-008-4739-0
- 1120 87. Becker JS, Mounicou S, Zoriy M V., Becker JS, Lobinski R. Analysis of metal-
1121 binding proteins separated by non-denaturing gel electrophoresis using matrix-
1122 assisted laser desorption/ionization mass spectrometry (MALDI-MS) and laser
1123 ablation inductively coupled plasma mass spectrometry (LA-ICP-MS). *Talanta*. 2008;
1124 76: 1183–1188. doi:10.1016/j.talanta.2008.05.023
- 1125 88. Karmakar S, Das KP. Identification of histidine residues involved in Zn²⁺ binding to
1126 α A- and α B-Crystallin by chemical modification and MALDI TOF mass spectrometry.
1127 *Protein J*. 2012; 31: 623–640. doi:10.1007/s10930-012-9439-0
- 1128 89. Jayasinghe SB, Caruso JA. Preliminary investigation of Cu-containing proteins in
1129 seeds of Brazil nuts by ICPMS and MALDI-MS methods. *Int J Mass Spectrom*. 2013;
1130 356: 33–36. doi:10.1016/j.ijms.2013.09.014
- 1131 90. Chen F, Gülbakan B, Weidmann S, Fagerer SR, Ibáñez AJ, Zenobi R. Applying mass
1132 spectrometry to study non-covalent biomolecule complexes. *Mass Spectrom Rev*.
1133 2007; 26: 223–257. doi:10.1002/mas
- 1134 91. Witkowska D, Politano R, Rowinska-Zyrek M, Guerrini R, Remelli M, Kozlowski H.
1135 The coordination of NiII and Cu(II) ions to the polyhistidyl motif of Hpn protein: is it
1136 as strong as we think? *Chemistry*. 2012; 18: 11088–99. doi:10.1002/chem.201200780
- 1137 92. Szájli E, Fehér T, Medzihradszky KF. Investigating the quantitative nature of
1138 MALDI-TOF MS. *Mol Cell Proteomics*. 2008; 7: 2410–2418.
1139 doi:10.1074/mcp.m800108-mcp200
- 1140

1141 **S1 Supporting Information**

1142 **Table S1. Proteins showing apparent SDS-resistant oligomeric forms upon denaturing**
1143 **SDS-PAGE.**

1144

1145 **Table S2. List of proteins retaining metal ion on SDS-PAGE.**

1146

1147 **Fig S1. Schematic diagrams of gene constructs and protein analysis by SDS-PAGE used**
1148 **for western blot and ELISA analysis.**

1149 A. Schematic diagram of gene construct consisted of *gfp* fused with artificial His.tag (left
1150 panel) and GFP-His6 protein expression confirmed by SDS-PAGE (right panel).

1151 B. Schematic diagram of *gfp* fused with *hpn* at C-terminal followed by stop codon (left panel)
1152 and recombinant protein of GFP-Hpn fusion analyzed by SDS-PAGE (right panel).

1153

1154 **Fig S2. Comparison of DNA sequence of *hpn* from *Helicobacter pylori* strain SS1 (this**
1155 **study) with strain 26695 (NCBI data).**

1156 The promoter region and *hpn* gene of strain SS1 was PCR amplified and nucleotide sequence
1157 was compared with NCBI data of strain 26695 (GenBank accession number U26361).

1158 Putative promoter elements are shown in a box. The *hpn* gene region is shown in uppercase
1159 letters and mutations at the nucleotide level are shaded in gray. The putative terminator region
1160 of transcription is underlined. The promoter region was highly conserved in strain SS1
1161 including Shine-Dalgarno sequence (GGAG) and promoter elements (-10 and -35).

1162

1163 **Fig S3. Separation of purified Hpn on non-denaturing blue native-PAGE.**

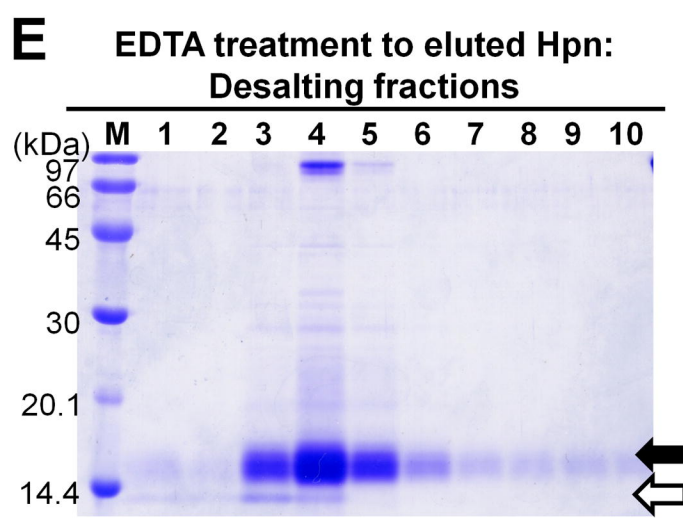
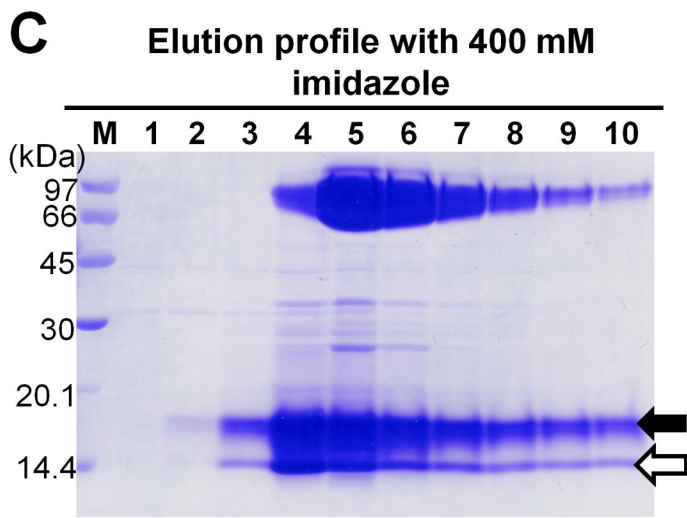
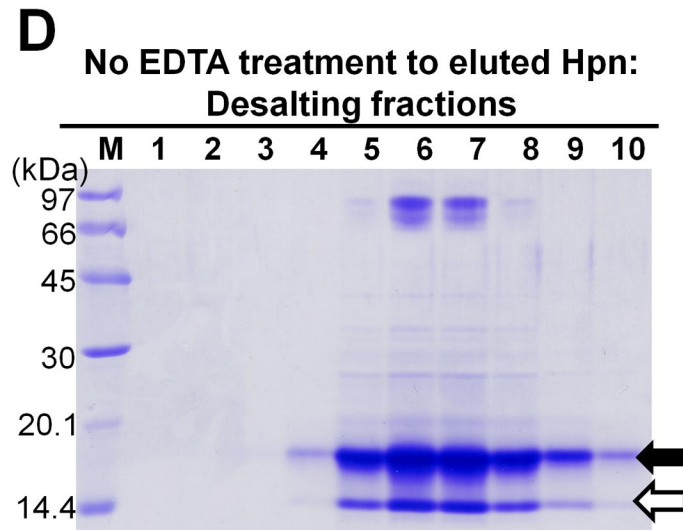
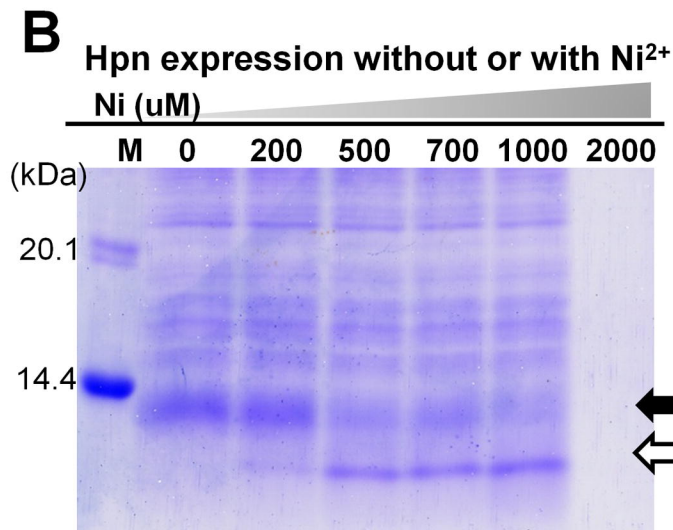
1164 High molecular weight marker (GE Healthcare), abbreviated as HMW, was used in all gels
1165 [Thyroglobulin (669 kDa), Ferritin (440 kDa), Catalase (232 kDa), Lactate dehydrogenase:

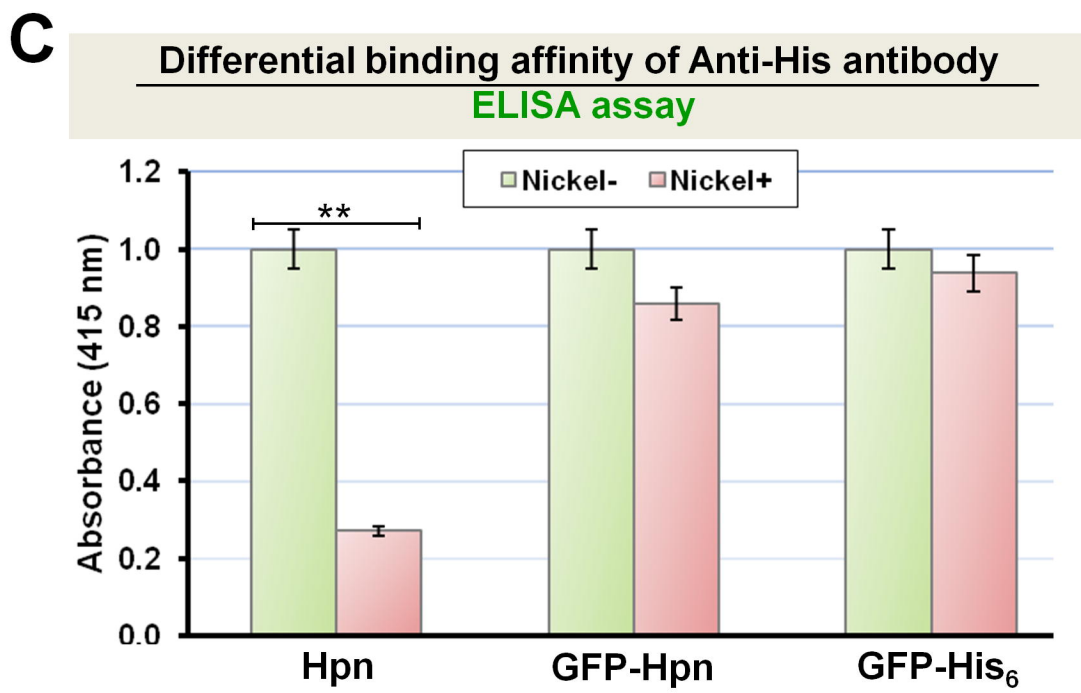
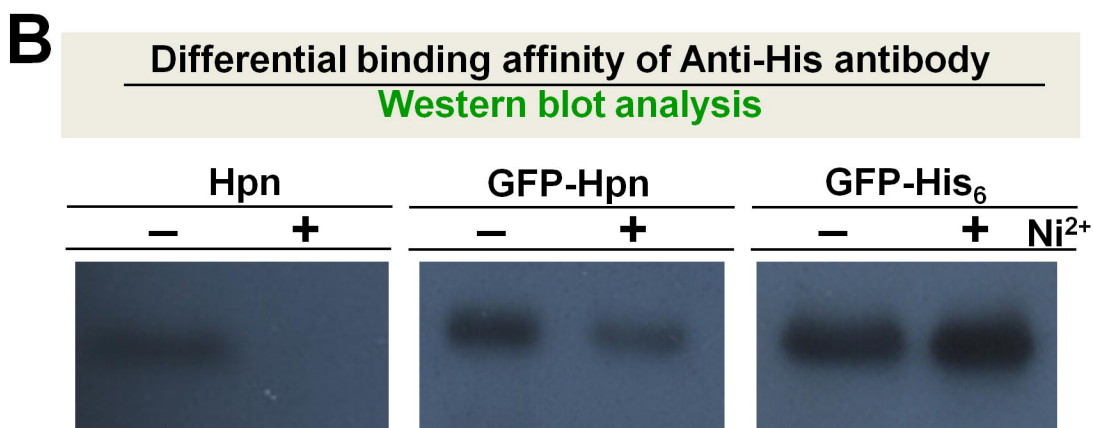
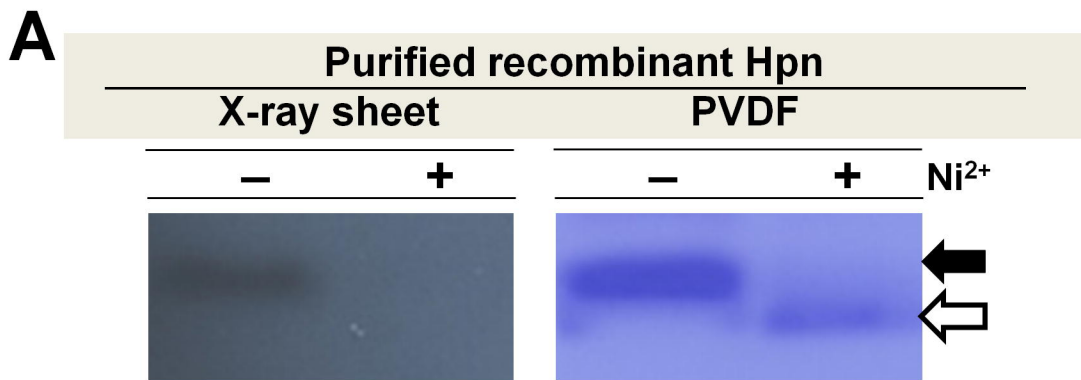
1166 (140 kDa) and Albumin (66 kDa)]. Recombinant Hpn (200 μ M) was treated with either 1
1167 mM of EDTA or Ni²⁺ independently and then applied to 10% native-gel. Apparent multimeric
1168 complexes of >670, ~500, ~230 kDa were observed in presence or absence of Ni²⁺ and EDTA.

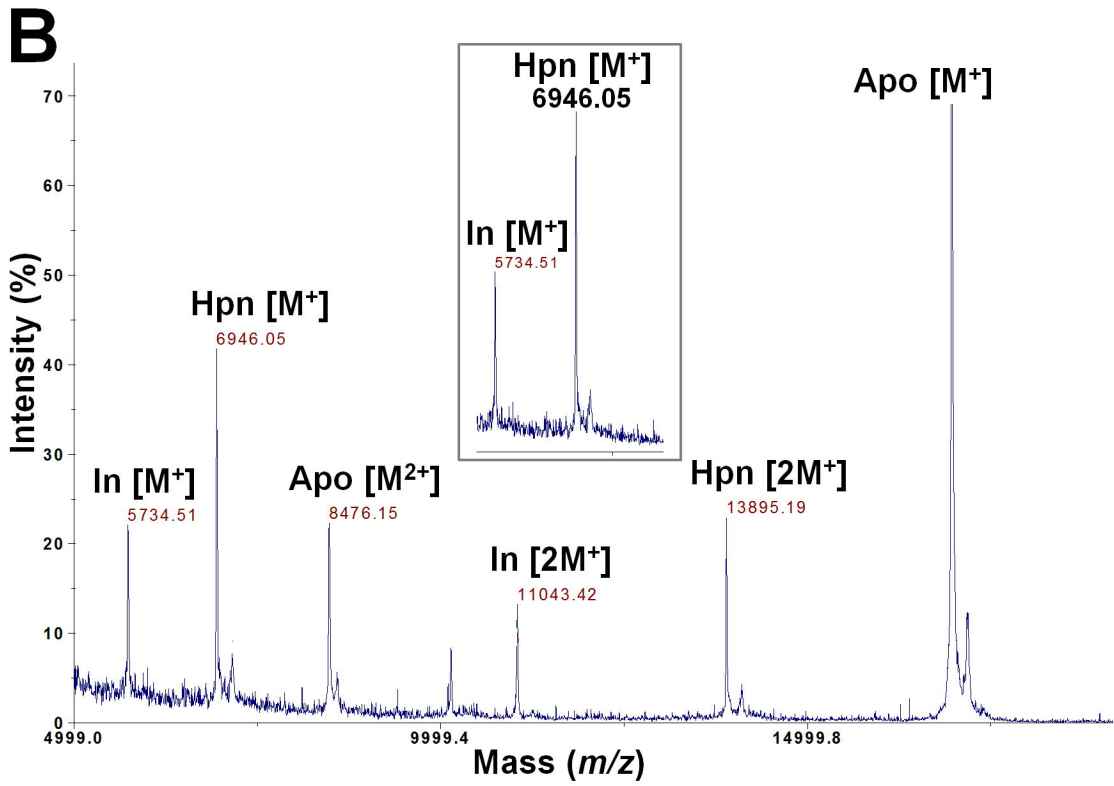
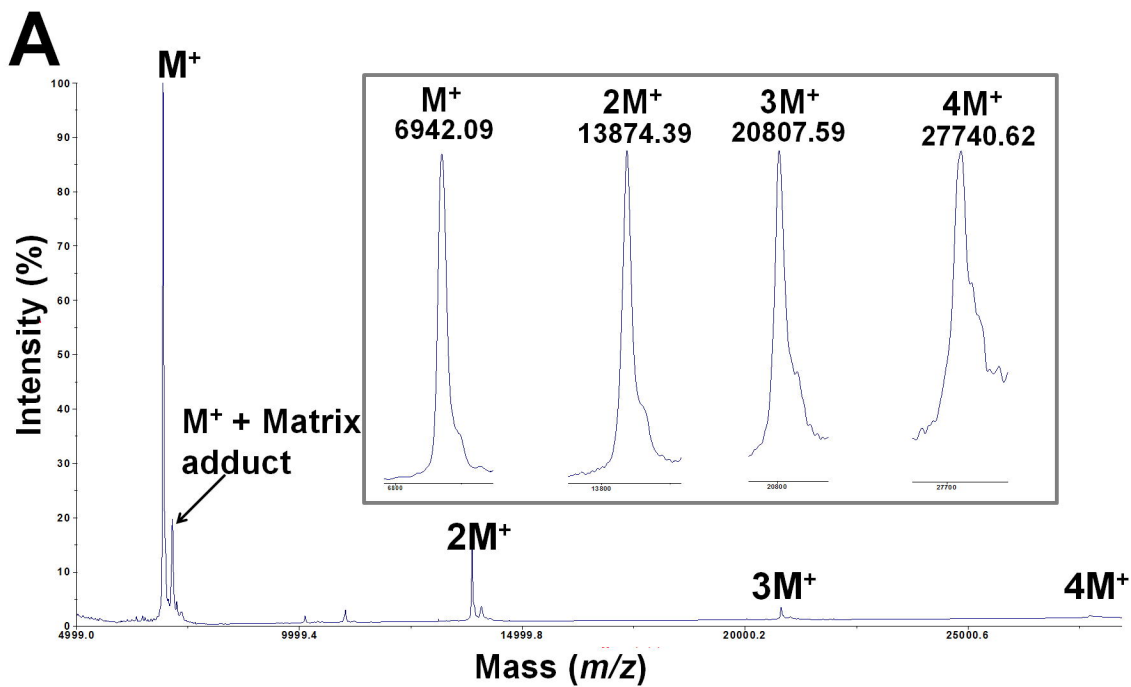
1169

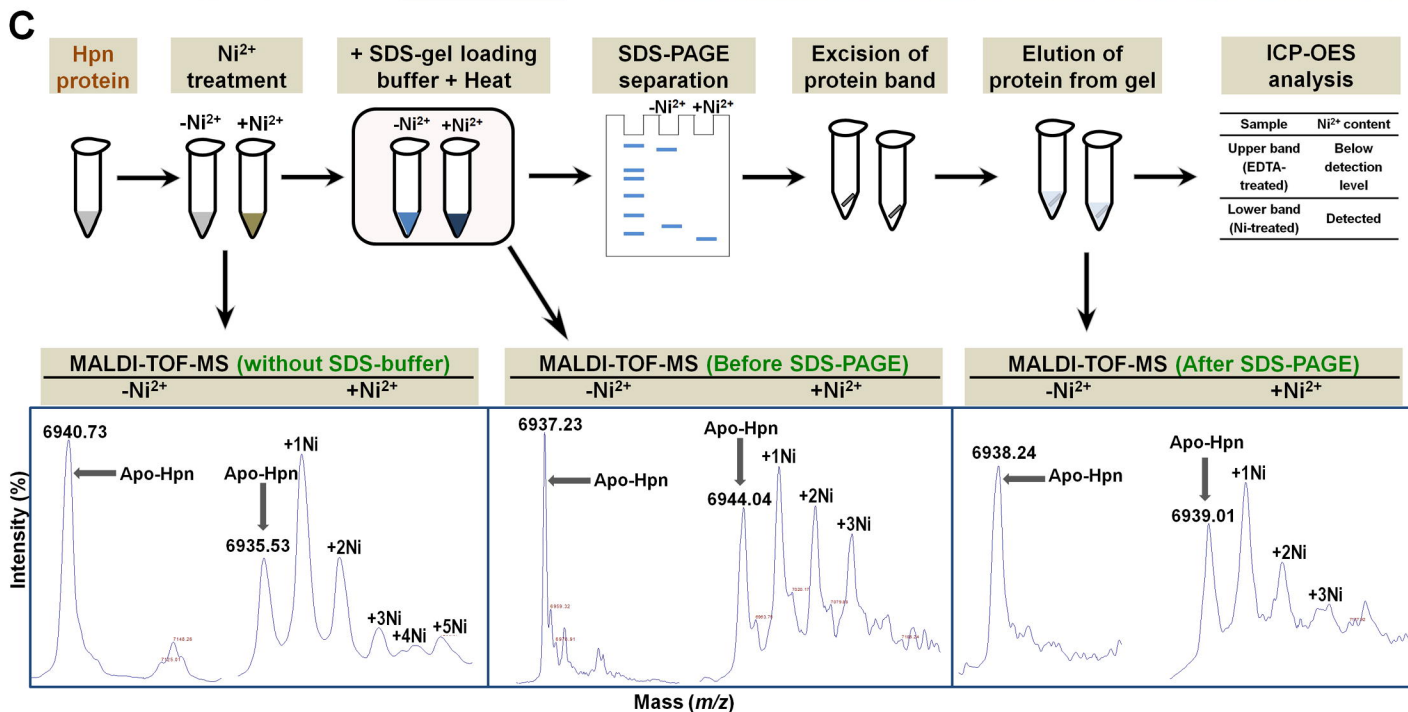
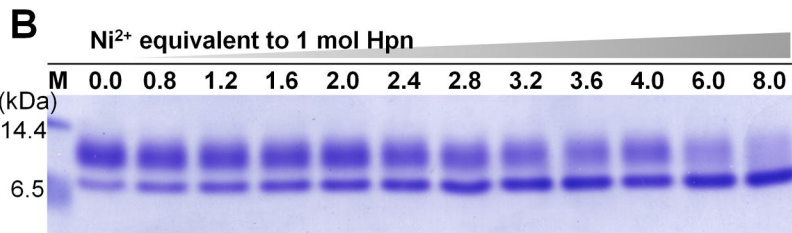
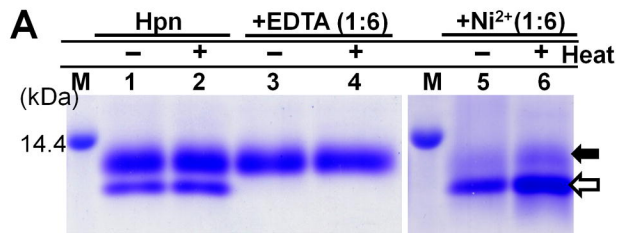
1170 **Annexure S1.**

1171 Protocol followed for analysis of apparent MW of Hpn on SDS-PAGE in Fig. 5.



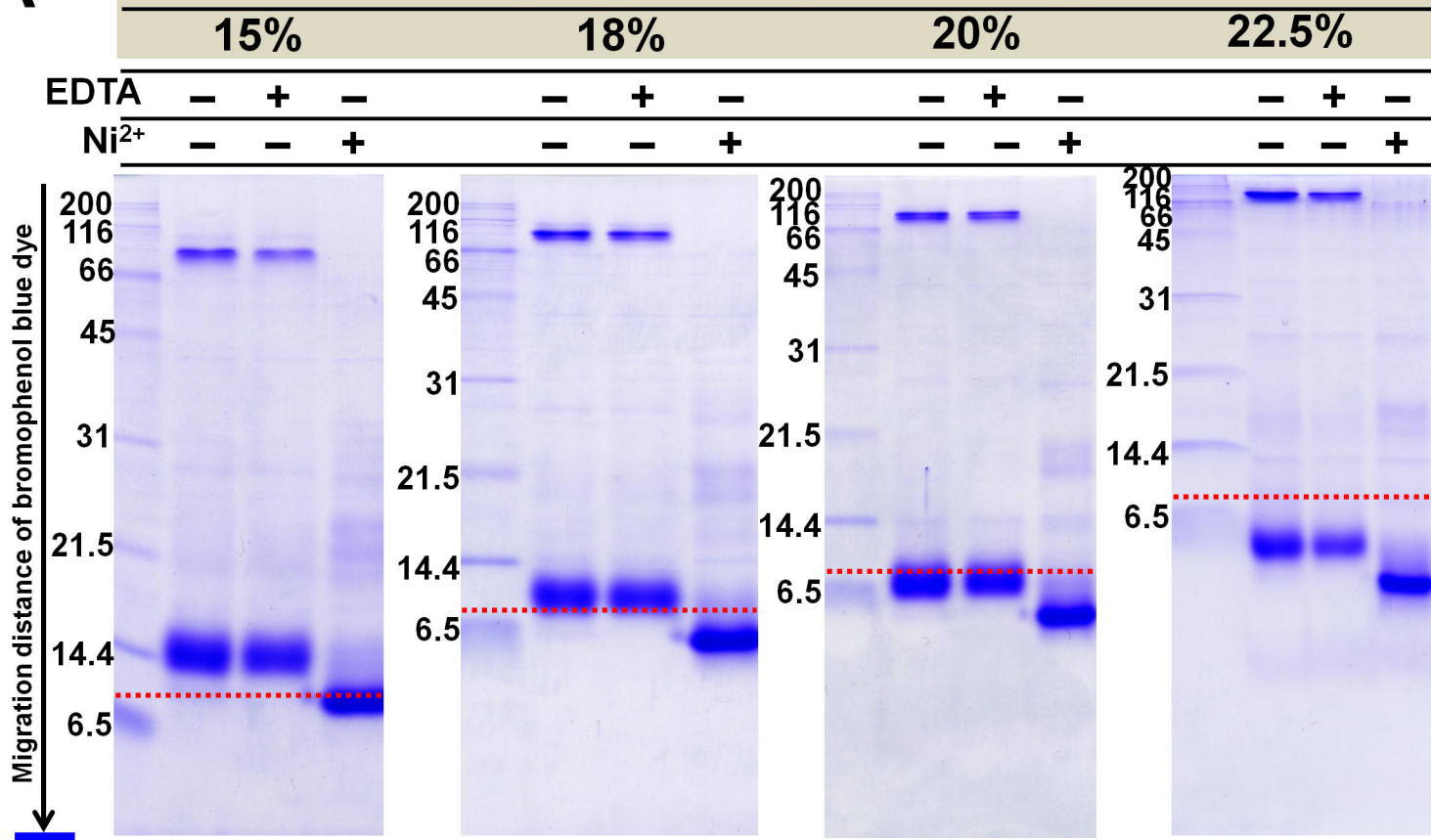




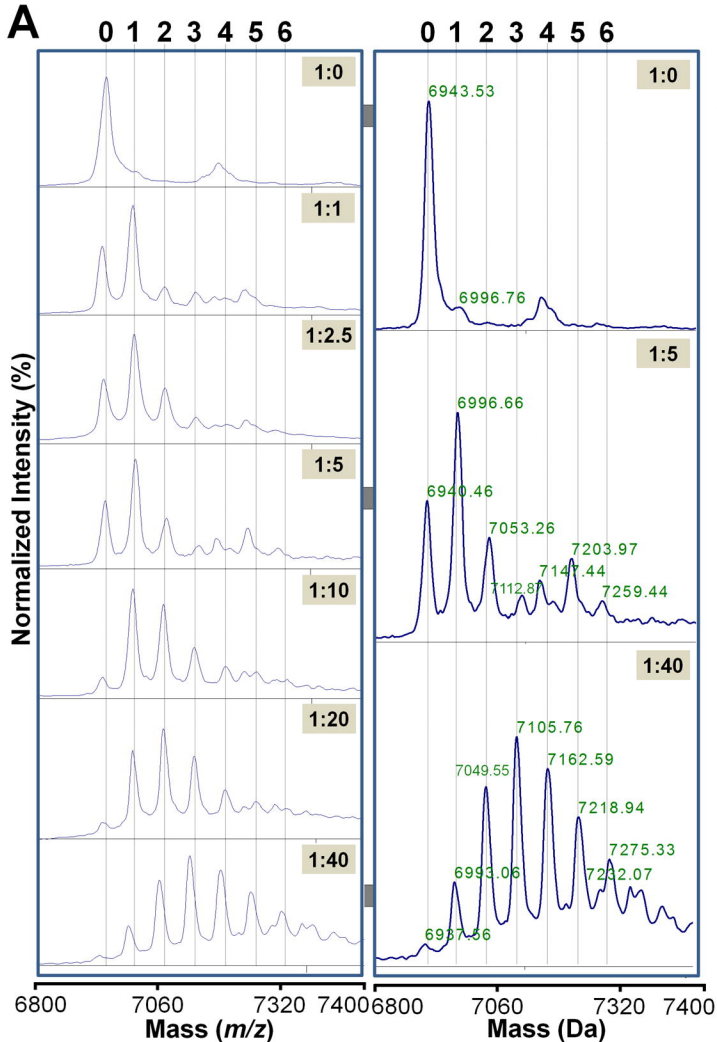


A

Polyacrylamide-gel percentage

**B**

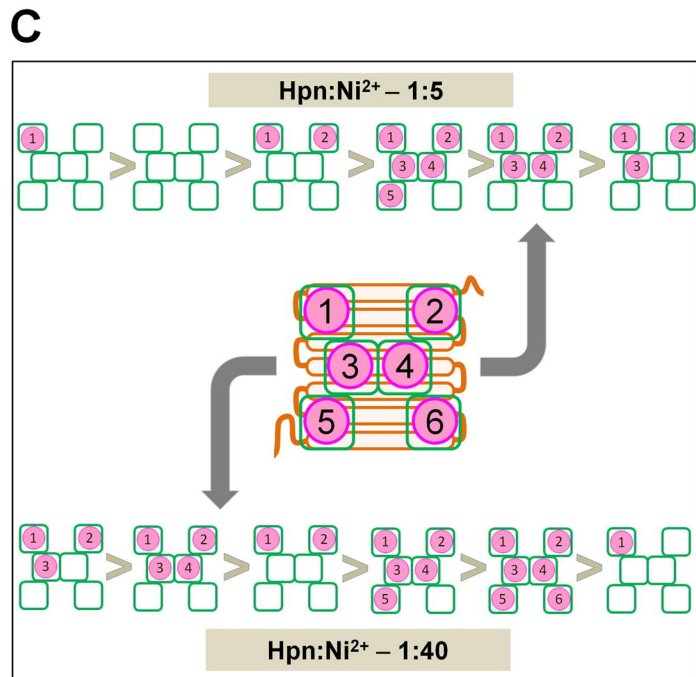
Polyacrylamide-gel	15 %	18 %	20 %	22.5 %
Apo-Hpn (kDa)	14.7	11.7	9.7	4.9
Ni ²⁺ -Hpn (kDa)	11.3	8.2	6.4	0.8
Difference between Apo-Hpn and Ni ²⁺ -Hpn (kDa)	3.4	3.5	3.3	4.1



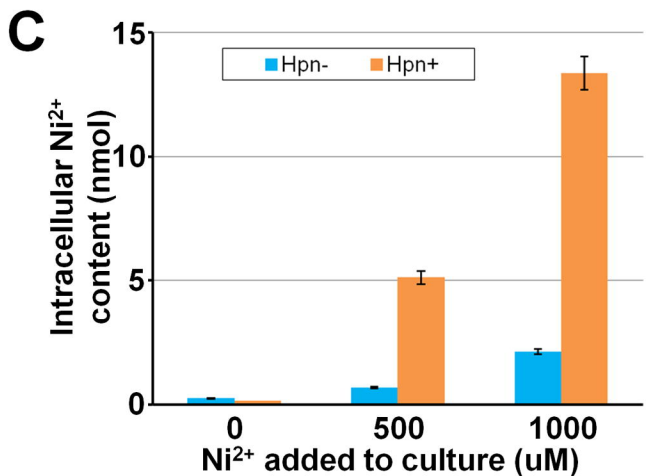
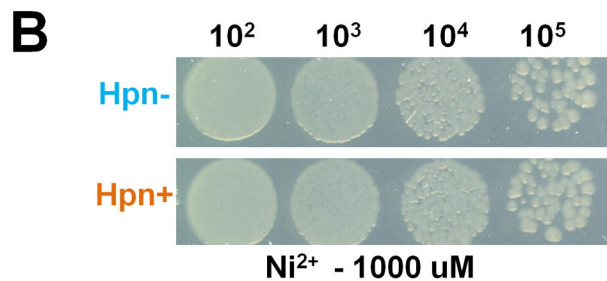
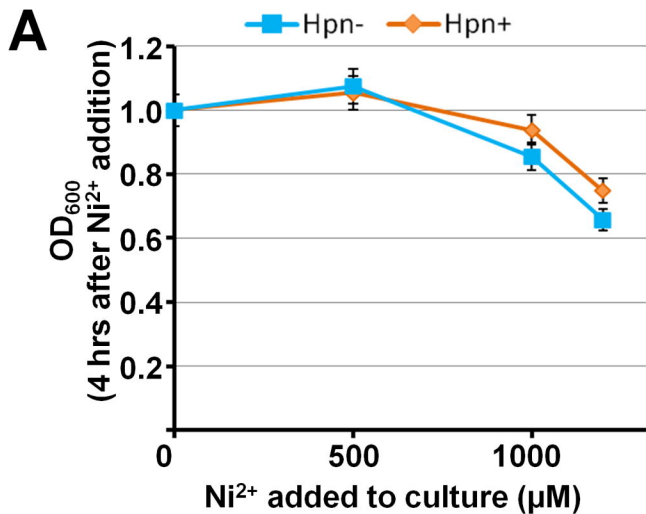
B

Mass difference between adjacent peaks

Label	0	1	2	3	4	5	6
MW	6937.6	6993.0	7049.5	7105.7	7162.5	7218.9	7275.3
Difference	-	55.4	56.49	56.21	56.83	56.35	56.39



Nutrient rich (LB) medium



Minimal (M9) medium

